Chapter 1

Introduction & Literature review with Experimental techniques

CONTENT OF CHAPTER

PART-A: Review and Scope of work

PART-A: Review and Scope of work

A1.1 Introduction

Human civilization is using a tremendous amount of energy to complete its day-to-day chores. To meet this required amount of energy, we are majorly dependent on fossil fuels (oil, coal, and gas). Generally, to derive the various forms of energy, non-renewable resources are converted into electrical energy. Moreover, this form of energy is very suitable for transmission, distribution, and control of energy, and due to this even the energy crunch in remote rural areas can mitigate easily. Energy consumption plays a pivotal role in the development of any country and even the literacy rate of a nation directly depends upon the per capita energy consumption. Therefore, an enormous amount of energy necessitates the augmentation of developing countries.

Since making available this ample amount of secure and sustainable energy is a huge challenge for mankind. In addition, it must be environmentally friendly and economically suitable forevery sector. Hence, the fossil fuel obvious could not be our promising candidate. From the prospect of economic side, the rising price of fossil fuels (petrol, diesel, and Kerosene) at an alarming rate is a major concern. Similarly, due to the consumption of fossil fuels, the emission of greenhouse gases and theiradverse effects like global warming and all on the environment has become a crucial point of consideration. The interconnected global warming and environmental pollution issues with the power generation infrastructures, including hydroelectric and thermal power, are real threats for society. Thus, we are critical in conjunction to play with ecology and sustainable developments towards a green environment [1].

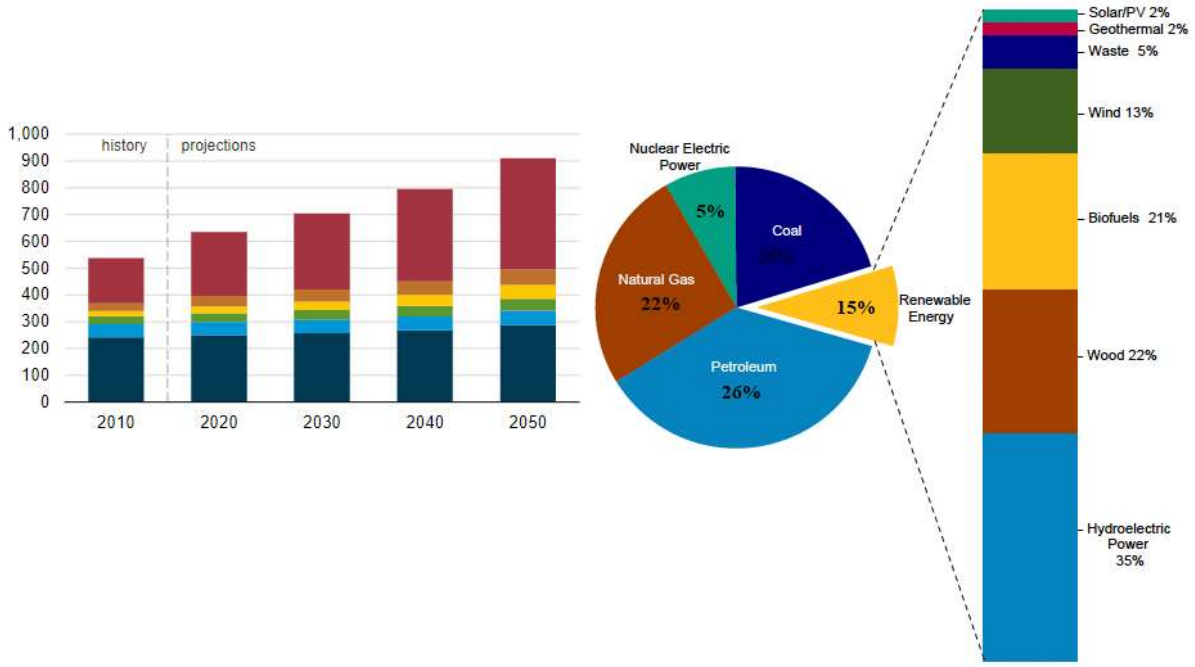

Fig.1.1: World energy demand and energy contributions from various energy resources [1].

In general, the contribution of non-renewable energy resources in total energy consumption is about 80% (Fig. 1.1), and soon it will be depleted due to the limited availability of required resources on the earth. Moreover, the various toxic gases and by-products which are generated after the consumption of renewable energy sources cause many serious problems for mankind like global warming, various respiratory problems, and many more. These adverse effects will continue to rise in the coming future and will also exacerbate our future generation. Therefore, this is the right time to focus on developing novel renewable energy sources to fulfill the high energy demand. Amid the critical energy crisis, there are varieties of renewable and non-renewable energy resources are available, and those are predicted to meet such vitality needs. According to the International Energy outlook 2019, the projected energy consumption, till 2050, will reach up to 911 quadrillions (BTU) [2].Various types of renewable energy technologies are available, which meet our energy requirement, such as wind energy, solar energy,

thermal energy, tidal energy, etc. The projected utilizations of these techniques are, depicted in Fig.1.2, indicating the contribution of renewable energy sources.

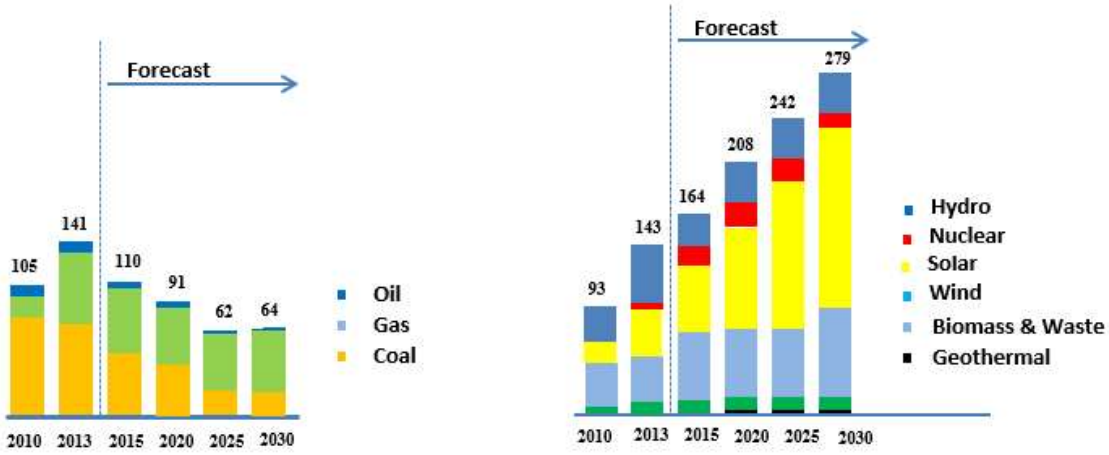

Fig.1.2: The contribution of non-renewable and renewable energy sources [3].

It is evident from Fig.1.2 that the contribution of renewable energy is increasing whereas consumption of fossil fuel decreases year by year. Among the available renewable sources, solar energy-based power generations are the fastest growing renewable source. Solar power generators possess various unique properties namely ease in energy harvesting, low installation cost, and better stability compared to other renewable energy sources. It is projected that the energy harvested by the sun itself has the potential to fulfill our energy demands. Whereas by avoiding the use of fossil fuels, we may reduce the harmful effect of energy production on the environment. Considering the harmful effect of fossil fuels, and the potential advantages of solar-based devices, most countries emphasize installing photovoltaic devices to save the environment globally. There is a pronounced surge of about 11% in the installation of PV solar systems from the year 2018 to 2019. In 2018, solar power stations with a capacity of around 512.3 GW were installed and in the following year, the number raised to 623 GW, after the installation of 112 GW

power systems in 2019. These installations were made by the International Energy Agency of Photovoltaic power system program (IEA-PVPS) countries and non-IEA-PVPS countries with a contribution of 509.2 GW and 113.4 GW, respectively. Regarding the installation and harvesting of solar energy, India stood at 4th position globally with the installation of 10.1 GW capacity power stationscountry-wide in 2019. China installed Solar-powered stations of capacity 30.1 GW, while in the United States installed 13.3 GW capacity solar stations in 2019 [3]. A pictographic representation of the worldwide production capacity of solar energy is depicted in Fig.1.3. The accompanying segment gives a concise overview regarding solar power or photovoltaic innovation over the years.

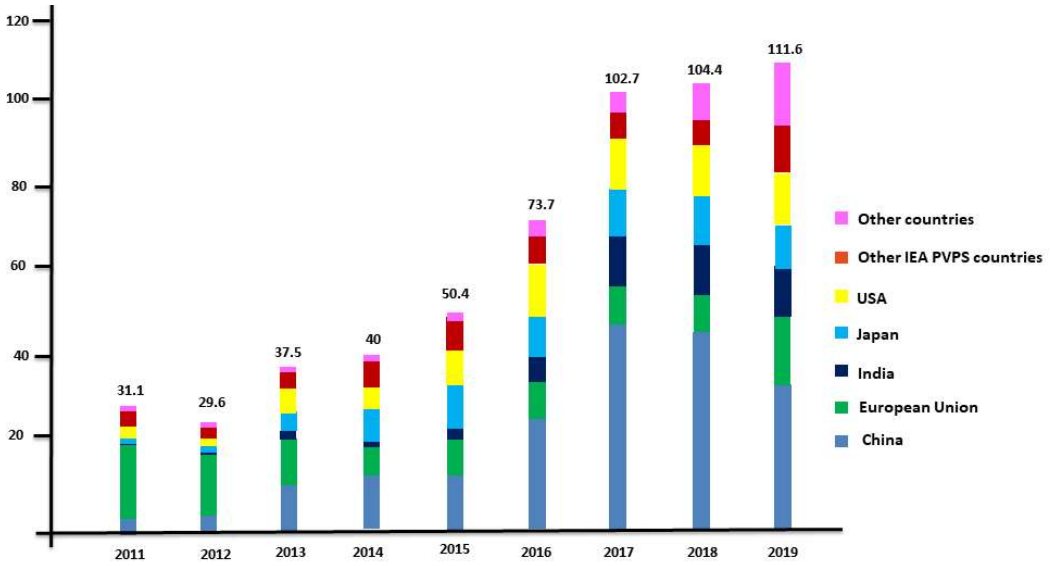

Fig.1.3: Development of PV generation capacity by IEA and non-IEA PVPS countries[4].

A 1.2 Motivation of Thesis

The economic factor is the principal challenge to develop affordable solar cells with high efficiency. Further, the development of reproducible, useful materials and device processing technology is critical parameter for the advancement of solar cell technology. The inter-related factors for industrial production flow-line, which directly affect the price

of the solar cells are the mass-production, improved cell efficiency, and affordable material cost [5]. The crystalline silicon (c-Si) material is expensive and costs maximum, in the silicon-based solar cell. For the fabrication of cost-effective solar cells, we need to develop technologies to make c-Si wafers thinner [6], wafer recycling [7], lower the costs of consumables, etc.[8]. Additionally, silicon recycling is also considered as one of the predominant concerns to make Si-solar cells affordable. It should be mentioned here that only a 10% increase in recycling of Si has been made over the last 10 years. The wafer recycling processes need to be more advanced and can be improved by developing appropriate recycling technologies [9]. The existing recycling technology uses a diamond sawing tool, which can lead in the future for the production of low-cost wafers [10]. It is evident that 40% of solar cells' expenses are attributed to the silicon wafer, so, for making cost-effective solar cells, companies need to use thin and ultra-thin silicon wafers in the fabrication of solar cells by integrating appropriate light management and passivation schemes. If the wafer thickness reduces, the Si-wafer photon absorption decreases since the absorbance varies as a function of the wafer thickness [11]. Similarly, the recombination losses also increase with reducing wafer thickness as the surface-to-volume ratio (S/V) increases [12,13]. The subsequent effect of less absorbance and increased recombination losses lead to reduce cell efficiency. However, it offers some advantages over conventional 180 μm silicon cells namely, it provides flexibility to the device, and it is feasible to integrate with roll-to-roll technology. To achieve the efficiency equivalent to the commercially available 180 μm solar cells, adequate optical engineering and light management schemes must be incorporated to counter the issues that arise due to wafer thickness reduction [14-16]. Additionally, it should also provide the passivation effect to the surface because more than 50-60% loss is due to recombination loss and these losses are significant at the surface. The issue of adequate wafer thickness to scale

the commercially available 180 µm wafer solar cell efficiency is very important. Shockley addressed the quest for adequate wafer thickness in 1985, and anticipated that a ~30 µm thick c-Si wafer is suitable for making efficient solar cells [17]. Further, a 30 µm thickness wafer also possesses good mechanical strength as well as facilitates easy free mounting of the solar cell. In 2018, the International technology roadmap for photovoltaic (ITRPV) had forecasted the significant reduction in the substrate thickness for the fabrication of mono-crystalline based single-junction solar cells for 2018-2028. According to their prediction, the thickness of the wafer reduces gradually from 180 µm to 140 µm [18]. Shockley reported that a ~30 µm thick c-Si wafer is sufficient enough to fabricate single-junction solar cells. This encouraged a group of researchers to develop new technologies for thin crystalline solar cells with both homo and heterojunctions.

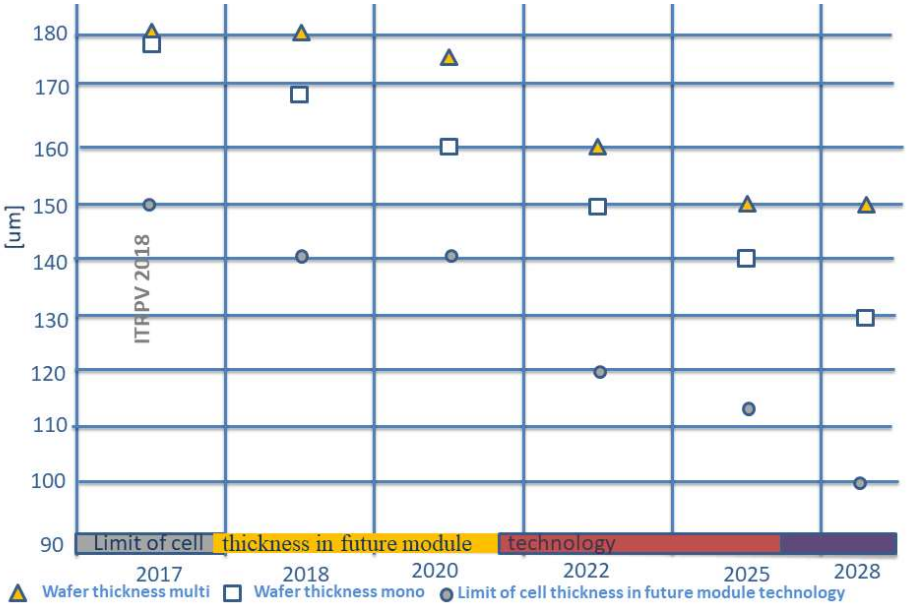

Fig.1.4: Predictions of the international technology roadmap for photovoltaic (ITRPV-2018) regarding the drastic lowering of substrate thickness in monocrystallinesingle-junction solar cells [18].

To prevent such a negative effect of the thin wafer, we must incorporate material layers that simultaneously act as a reflector as well asa passivator. The material whose *"k"* value is approximately zero is suitable for reflector and surface passivator at the same time.

Numerous materials and their stacks that have been investigated (such as SiO_2 [19,20], HfO_2 [21,22], Al_2O_3 [23,24], ITO [25,26], SiN_x [27,28]) and widely used by the scientific communities for optical engineering the solar cell via surface-passivation [29-31]. The appropriateness of these materials depends upon various factors such as their UV stability and thermal stability. In addition, the most preeminent is the light absorption in the wavelength region relevant for the solar cell operation. The surface passivation depends upon the type of charges (-ve or +ve) formed by the layer, density, type of dopant, etc. The following section summarizes optical and passivation properties of the above-mentioned materials:

i) Silicon dioxide (SiO_2)

Silicon dioxide (SiO_2) provides a high-quality interface to the Silicon surface when it is thermally grown. The interface charge density (D_{it}) of SiO_2 is below 10^{10} $cm^{-2}eV^{-1}$ [32] and the effective surface recombination velocity (S_{eff}) is below 10 cm/s [33,34]. Therefore, SiO_2 offers a high degree of chemical passivation in comparison to the field-effect passivation. It is also valid for both n &p-type semiconductors and true for a wide range of doping [35, 36].

ii) Silicon Nitride (SiNx)

Silicon nitride has been widely used as a preferable dielectric in the c-Si solar cells [37]. It behaves as an antireflection layer and a surface passivation layer in a c-Si solar cell (at the front n^+ emitter layer). The quality of passivation depends upon the concentration of N_2, H_2 gases, and Si precursors while depositing on the surface of silicon [38]. In the presence of hydrogen gas concentration, good quality (more than 10-15%) of passivation is obtained to date [39]. For example, if the N_2 gas concentration is kept lower concerning other gases, the as-grown silicon nitride layer, provides chemical passivation, whereas the layer provides field-effect

passivation (with high fixed charge densities around 10^{12} cm^{-2}) if N_2 concentration is high [40-41].

iii) Aluminum Oxide (Al_2O_3)

Al_2O_3 layer provides a high degree of passivation to c-Silicon. Due to the formation of a high-density negative charge on the film, and its ability to decrease the density of the interface state [42,43], Al_2O_3 is well-known for providing excellent passivation among all the materials. In specific, Al_2O_3 exhibits perfect passivation properties when it is deposited using PECVD and deposition techniques[44]. The Al_2O_3 passivation provides 20.6% and 23.2% efficient passivated emitter rear contact passivated emitter and rear contact (PERC) and passivated emitter with rear locally diffused (PERL) solar cell [45]. It was reported that the thin nano-scale Al_2O_3 layer deposition, using ALD, yields ~25% efficiency in PERL solar cells [46].

iv) Hafnium Oxide (HfO_2)

HfO_2 is one of the most important dielectricmaterials that have a high- K dielectric constant anditis widely used in the microelectronics and solar photovoltaic industry. It is well-explored material and high quality HfO_2 can be deposited by ALD. HfO_2 generally provides the field-effect passivation by forming positive and negative fixed charge density at the interface [47]. In the HfO_2 layer, the charged and neutral oxygen vacancies act as trap centers, and they are primarily responsible for the fixed charges [48,49]. Also, oxygen vacancies can trap the electrons, which results in a net negative charge after external perturbation [50].

Compared to the single-layer mentioned in previous texts, stacks of two or more layers often be used where; we can get farmore beneficial properties compared to the single layer. The deposition of one more layer helps to improve passivation properties as well

as optical properties. By manipulating the thickness of stack layers we can precisely tune the passivation properties and optical properties associated with it. The appropriate combination of the dielectric layers on Si provides a *charge tailoring*. Charge, which provides passivation in the form of field-effect, can be changed from positive to virtually zero or the strong negatively charged states [51, 52]. In the same manner, optical trailing can be performed for increasing the reflectance and decreasing the transmittance at the back of the solar cell. Defects in a dielectric that are adjacent to Si can be engineered or designed for increasing or decreasing the built-in charge that can repel the same kind of charges from the vicinity of the surface [53]. These innovative ideas in point-defect engineering further improve the passivation quality while increases reflectivity aids to enhance the solar cell performance. It should be mentioned here that the very popularly used useful dielectric stacks are prepared using various layers, includingAl_2O_3, SiO_2, HfO_2, Si_3N_4, and ZnO.

A1.3 Objectives of the thesis

Because of the aforesaid motivations, the following significant objectives were set to address in the present thesis.

- Fabrication of thin and flexible crystalline silicon solar cells based on the single-junction concept with the help of ~30 μm (instead of 180 μm) thick c-Si wafer.
- Improvement of the theoretical optimization of light reflection capabilities for two different types of dielectric stacks, viz. SiO_2/Al_2O_3 and HfO_2/Al_2O_3withdifferent thicknesses need to be carried out using COMSOL Multiphysics™ software based on finite element method (FEM) numerical solution technique.
- Fabrication of efficient Silicon heterojunction (SHJ) solar cell with notable high efficiency.

- Fabrication of ITO/ZnO:ZnMgO nanopillar)/PCBM/P3HT:PCBM/PEDOT:PSS/Ca-Al based heterojunction organic solar cells.

A1.4 Evolution of Solar cell

A solar photovoltaic cell or solar cell is a device based on semiconductor materials that use to translate the incident solar energy into electrical energy. The research in the field of solar cells is progressed after the discovery of the photovoltaic effect i.e.voltage will develop when semiconductor material is exposed to sunlight. This effect was first proposed by French scientist *Edmond Becquerel* in 1839 [54]. The initial observation of the photovoltaic effect was reported in an electrolytic cell, which comprises two platinum electrodes coated with silver chloride, immersed in an acidic medium, resulting in the generation of voltage and current when exposed to sunlight. After more than 30 years of such reports, *Willoughy Smith* observed a similar effect in the selenium element [55]. In the year 1894 first solar cell was developed by *Charles Fritts*, with 1% efficiency, and of course, this small efficiency cell is not suitable for usable device application. With the advent of semiconductor technology, in the year 1954, three scientists of Bell Labs USA *Pearson, Chapin,* and *Fuller* developed a p-n junction-based solar cell with an efficiency > 4% [56,57]. This discovery was a breakthrough in the field of photovoltaics. The as-developed cell consists of lithium as a doping element for making junction rather, it is replaced by boron doping that raises the efficiency of the cell from 4% to 6% [58]. The current technology of silicon solar cells is following the trend shown by this discovery. With the advent of silicon technology, silicon solar cell efficiency also increased. In 1970's, the Silicon solar cell's efficiency increased to 14%, and solar cells found an immediate application for space missions [59, 60]. Later on, significant improvement in

solar technology has been reported due to the tireless comprehensive efforts of academic institutes and research laboratories. Till now, overall, around 400% increment in efficiency is achieved. In solar cell research not only limited to silicon elements but also few other materials were explored, such as amorphous silicon (a-Si), Cadmium Telluride (CdTe), Cadmium Sulphide (CdS), Gallium Indium Phosphide (GaInP), organic, inorganic, organic-inorganic hybrid, perovskite, etc. [61-68]. These materials are suggested for a potential alternate to silicon, and are extensively explored. These materials are used for application in advanced solar cells. The choice of the material decides the stability, cost, and conversion efficiency of the fabricated devices. Fig.1.5 depicts the trend the power conversion efficiency trends achieved with various types of solar cell technologies.

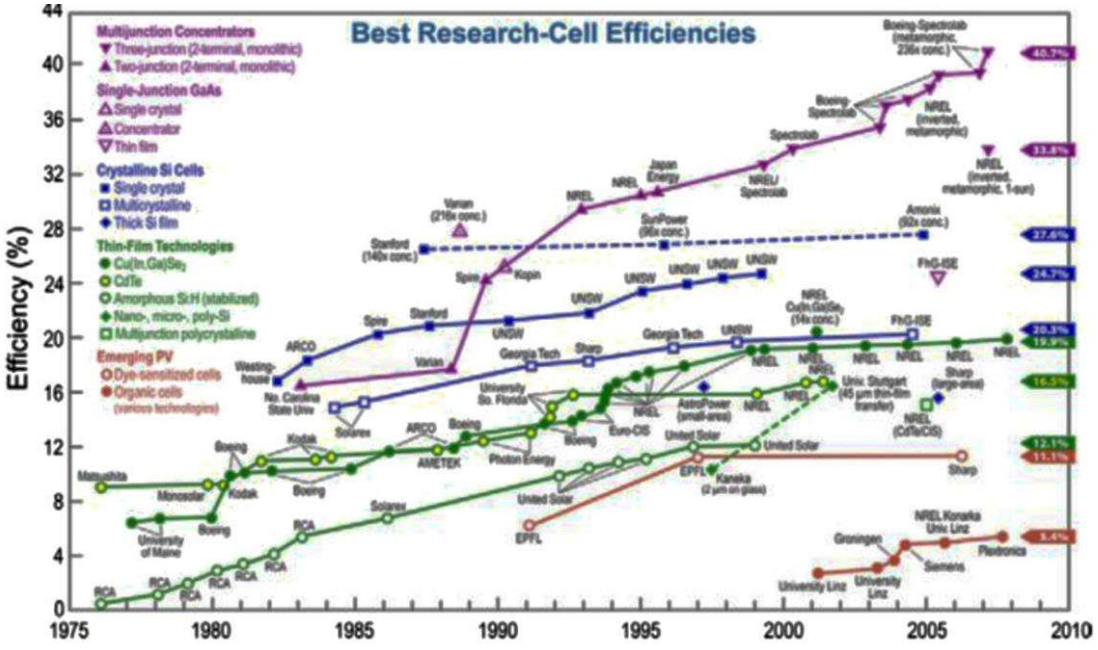

Fig.1.5: Efficiency improvement of different types of research on solar cells over the years (Reproduce with permission of Elsevier) [69].

A1.5 Generations of Solar cell

During the last 70-80 years, numerous solar cells have been developed and classified according to the active or absorbing material used to fabricate the device. Broadly, a solar cell is categorized into three different types, as depicted in the flow chart (Fig.1.6).

1.5.1 First Generation

The solar cell manufactured from c-Si/III-V group semiconductor solar cell known as the first generation solar cell. The function of this generation of solar cells depends on its active material or absorbing materials, which are III-V semiconductors such as silicon, Indium phosphide/gallium arsenide (GaAs), Indium phosphide(InP), etc. Further, it is bifurcated into two categories i.e., single junction and multi-junction solar cells. In a single junction, only one type of absorbing material like GaAs/InP or mono/multi c-Si and one p-n junction is used. Generally, in a single junction solar cell same material is used for fabricating p and n layers, whereas, in a multi-junction solar cell, one or more semiconductor (p-n) junction is incorporated with different active absorbing materials. These different active absorbing materials are arranged in decreasing bandgap from top to bottom to facilitate the charge flow. Some examples of single-junction first-generation solar cell are mono & multi c-Si solar cell, InP/GaAs solar cells, whereas examples of multi-junction solar cells are GaInAsP/GaIn(double junction), GaInP/GaAs(double junction), GaInP/GaAs/InGaAs(triple junction), GaInP/GaAs/GaInAs/GaInAs (four junction), etc.

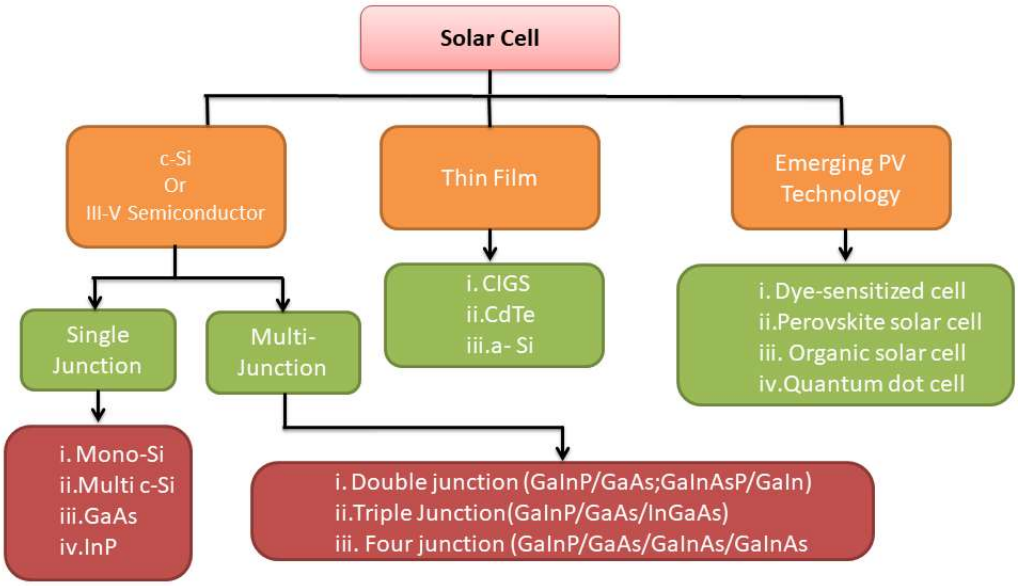

Fig.1.6: Schematics of solar cell classification.

1.5.2 Second Generation

A separate category of solar cells is referring as *thin-film solar cells* or second-generation solar cells. In this type of cell, active material thickness is composed of few microns, and the p-n junction is made of identical as different kinds of materials. If both, p-type & n-type materials, are identical then the device is referred as homojunction, whereas, if the materials are different the device is referred as a heterojunction device. Examples of second-generation solar cells are Copper Indium Gallium Selenide (CIGS), Cadmium Telluride (CdTe), and hydrogenated amorphous silicon (a-Si:H), etc.

1.5.3 Third Generation

The emerging PV technology is categorized as the third generation of solar cell technology. A few examples of the third generation of solar cells are dye-sensitized solar cells, perovskite solar cells, quantum dot (QD) solar cells, organic solar cells, etc. In a dye-sensitized solar cell, *Rutheniumpolypyridine* [70] dye, PCBM, P3HT, or their blends [71] are preferably used as active materials. In quantum dot solar cells, nano-sized materials like PbS, CdTe, etc., are used as an absorbing material [72,73]. The perovskite

solar cell use materials like methylammoniumleadtrihalide ($CH_3NH_3PbX_3$) (X=halogen) [74].

The solar cell device is a semiconductor-based device, which performance is affected by the quality of material, ambiance conditions, fabrication and optimization techniques, etc. Hence, it is important to pay attention to the parameters associated with the solar cell which ultimately affect the efficiency. The solar cell efficiency effectively depends upon four major factors: short circuit current (J_{sc}), open-circuit current (V_{oc}), fill factor (FF), and loss mechanisms. The brief discussion is given in the following texts:

A1.6 Photovoltaics process and Important parameters

1.6.1 Photovoltaics process in solar cell

The overall solar cell operation includes critical optical and electrical processes to convert solar energy into electric energy. The major background processes are as follows:

i. Solar photon absorption;
ii. Charge generation;
iii. Charge separation;
iv. Charge transportation.

1.6.1.i Solar photon absorption

When a solar photon impinges on the upper active layer of the solar cell, it may get absorbed and induce electron from the valence band (VB) of layer material to move in the conduction band (CB). This electronic transition (VB to CB) is subject to the adequate photon energy $h\upsilon > E_g$ (wavelength $\lambda < hc/E_g$) required to produce free electrons and holes. The photon absorption is quantified by the universal parameter absorption coefficient "α". Absorption coefficient estimate by the following relation:

$$N_t = N_0 \exp(-\alpha x) \quad (1.1)$$

where N_t and N_0 is the number of photons at the given time after and before the light incidence, respectively. The term "x"represents the path length in the semiconductor. Further, with the reduction in path length or thickness of the wafer, photon absorption reduces. One should wisely select the semiconductor element having a bandgap comparable to the incident photon energy. To utilize a full working solar spectrum, absorbent material should possess a significant extinction coefficient (0.0189 for c-Si), in addition to that, it may have a small bandgap (~1.1 eV for Si) and appropriate Fermi level position.

1.6.1.ii Charge generation

The photon absorption leads a generation of electron-hole pairs (EHPs), and the rate of EHP generation per unit volume per unit time $G(x)$ is given as:

$$G(x) = -\frac{dN_{ph}}{dx} = \alpha N_0 \exp(-\alpha x) \quad (1.2)$$

1.6.1.iii Charge separation

The subsequent event after generating electron-hole pair is the extraction of charges immediately before they recombine. Recombine may avoid by creating asymmetry in the structure. The charge separation may be accomplished by an electric field that drifts electrons and holes into the opposite directions. The better dissociation of charge carrier (electron and hole) in the opposite direction may achieve by effective arrangement of band structure and proper alignment of Fermi level.

1.6.1.iv Charge transportation

Transportation of charge-carrier to the contact electrodes is a very crucial process. The adequate charge carrier transportation to the contact is subject to high carrier lifetime (τ), considerable diffusion length (L_d), high mobility (μ), etc. For that purpose, proper selection of electrodes is necessary.

A 1.6.2 Important solar cell Parameters

1.6.2.i Short-circuit current (J_{SC})

This current is the maximum current attain by the solar cell when its terminals are short-circuited. Factor J_{SC} depends upon the semiconductor (SC) bandgap expressed by the following relation :

$$J_{SC} \alpha \frac{1}{Band\ gap\ of\ SC}$$

Numerically, J_{SC} is calculated by integrating the photon flux within a limit of the highest photon energy to the cut-off energy level (bandgap of the SC) and multiplied by elementary charge q (1.6×10^{-19} C).

1.6.2.ii Open-Circuit Voltage (V_{OC})

Open-circuit voltage is the maximum voltage obtains across the solar cell when its terminals are open. The open-circuit voltage, V_{OC} is decided by the semiconductor bandgap, and the upper limit of the V_{OC} is equivalent to the semiconductor bandgap. Further, V_{OC} indicates the potential level difference of the contacts (quasi-Fermi level of the SC), which sets the upper limit of the V_{OC} of the solar cell. Mathematically, it is expressed by the following relation

$$V_{OC} = \frac{kT}{q} \ln\left(\frac{I_L}{I_0} + 1\right) \qquad (1.3)$$

where, I_L and I_0 are the load current under illumination condition and the recombination current, respectively. The high V_{OC} can be achieved by the keeping I_0 small [5].

1.6.2.iiiEfficiency (η)

The efficiency of a solar cell is defined as its ability to convert the solar photon into electricity and is expressed as follows [55]

$$\eta = \frac{V_{OC} \mathrm{I_{SC}} (\mathrm{FF})}{\mathrm{P_d}} \qquad (1.4)$$

Where, V_{OC} is the open circuit voltage, I_{SC} is short circuit current, FF is fill factor of the cell and P_d is solar photon density coming from the sun.

1.6.1.iv Fill Factor (FF)

The fill factor depends upon the value of series and shunt resistances of the solar cell. Series resistance comprises the emitter, base, and metal-semiconductor contact resistances that occur in the path of the cell. The shunt resistance is due to the leakage across the p-n junction, and it includes the periphery of the device, crystal defects, and impurities at the intersection. For an efficient solar cell, series resistance should be low, where as shunt resistance should be high. The fill-factor is given by [5]

$$FF = \frac{v_{oc} - \ln(v_{oc} + 0.72)}{v_{oc} + 1} \quad (1.5)$$

Where v_{oc} is $V_{OC}/(kT/q)$

A1.7 Loss mechanism in Solar cells

In solar cells, silicon material is a well-studied and explored topic among scientific communities. Efforts have been made to stimulate maximum performance; however, it is yet to be achieved. Notably, *Shockley-Quisser*s calculated the maximum possible conversion efficiency of solar cells, which is ~30% [17]. While considering various loss factors, the maximum conversion efficiency in mono and multi-crystalline silicon solar cells is 21% and 18%, respectively [75]. The newly reported passivated emitter rear locally diffused (PERL) cell achieved 25% conversion efficiency against the highest theoretical conversion efficiency of ~29% [76,77]. The following segment addresses the various losses in the solar cell Fig.1.7 depicts the various loss mechanisms in solar cells.

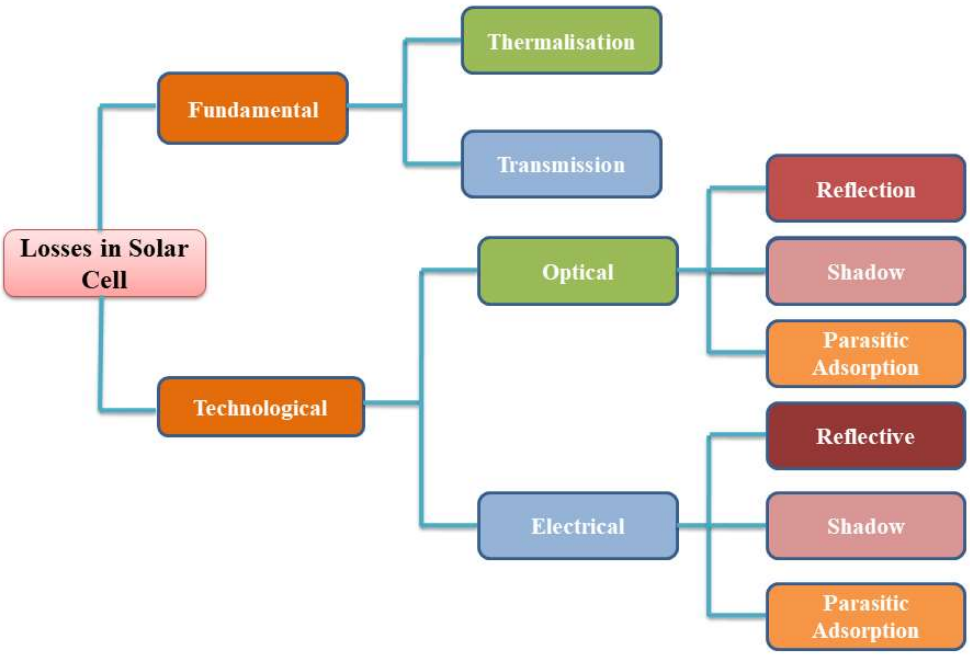

Fig.1.7: Different types of losses in solar cells.

1.7.1 Fundamental losses

This loss is due to the bandgap of the semiconductor, and it is further classified into two categories.

1.7.1.iThermalization loss

When a photon incident on the silicon substrate, which has energy more than the Si-bandgap (BG), the electrons absorb the energy and undergo transitions from the valance band to the conduction band. The excited electrons instantaneously lose their energy in the form of heat and fall at the edge or lower level of the conduction band. Therefore, the photons having energy more than the bandgap of the semiconductor laid to the thermalization losses, in the material. It is because of the partial energy of the photon, which is used for electronic excitation, and the remaining energy is released in the form of heat.

1.7.1.ii Transmission loss

Transmission loss is one of the significant parameters which directly influence the conversion efficiency of the solar cell. It depends upon the bandgap as well as the

thickness of the absorber material. The photons, having energy less than the absorber material's bandgap, will not get absorbed by the material and are unable to contribute to EHP generation and escapes from the wafer. Nevertheless, if the thickness of the absorbing material or wafer is further decreased, the transmission loss will also increase. Moreover, in the case of ~30 μm thin silicon, the transmission loss is very dominant compared to other losses, as it absorbs the wavelength upto 680 nm. The rest of the radiations of the solar spectrum (300-1100nm) transmit out from the wafer. These types of losses can be minimized by adding dielectrics, nanomaterials, nanostructures at the rear side of the solar cell [78-80]. These additive layers induced transmitted light to undergo multiple bounces, scattered and subsequently increases the path length leading to the possibility of re-absorption.

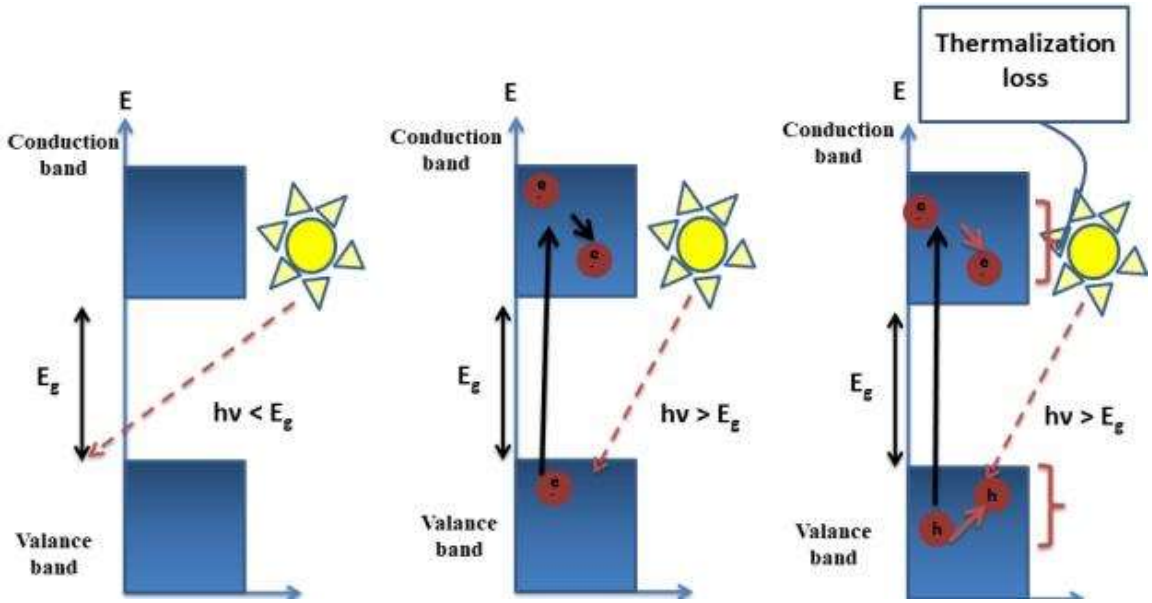

Fig.1.8: Schematics of fundamental losses in silicon solar cells.

1.7.2 Technological losses

1.7.2.i Optical losses: The major optical losses in a solar cell are given as follows:

1.7.2.i.a Reflection loss

The major contribution of optical losses in a solar cell is due to the reflection of incident light. The reflection loss originates from the reflection of incident light which

falls on the device, from every possible direction, at the front as well as rear surface. In a normal case 30% light is reflected from the bare silicon wafer [81] and this can be reduced by the front surface texturization. The texturization brought down the reflection loss upto 11%; antireflection coating and the combination of both may reduce the loss upto 5% [82].

1.7.2.i.b Shadow loss

For the efficient extraction of electrical power generated in solar cells, metal contacts must be created at the front and rear sides. The metal contacts reflect the light which is falling on the solar cell leading to reduce the current (I_L). This loss may be minimized, up to some extent, by fabricating fine contacts on the front side of the cell [83].

1.7.2.i.c Parasitic absorption loss

The parasitic absorption loss is attributed due to the light absorbed by the cell but not used to generate electron-hole pairs. The un-utilized light results decrease in photocurrent due to band-to-band absorption.

1.7.2.ii Electrical loss

Electrical loss is a crucial loss that directly affects the conversion efficiency as well as fill factor of the cell. Broadly, there are two types of such losses as given below.

1.7.2.ii.a Losses due to recombination

When light falls on the surface of the solar cell, light is absorbed by the bulk material, resulting electron-hole pair which is separated by a built-in-electric field present in the depletion layer. The separated charge is collected by the metal contacts at the front and rear ends.The maximum efficiency may be achieved, only, in that case when all the photo-generated electron-hole pairs will be collected by the metal contacts. Hence, all photo-generated electron-hole pair is unable to contribute in generating current and

voltage. This happens due to the recombination of charges. There are many regions in the solar cell where these generated charge carriers may recombine and the efficiency of the device compromise. The probable regions of recombination are the depletion region around the junction, emitter regions; depletion regions, front and rear surface regions, etc.

1.7.2.ii.b Loss due to the parasitic resistance

The parasitic resistance includes series as well shunt resistances which affect the fill factor (FF) and in turn affect the efficiency of the cell. In solar cell series resistance comprises the sum of all electrical components which occur in the path of the current flow. It includes semiconductor-metal contacts, base-emitter, and metal contact resistance. For higher efficiency, the value of series resistance must be as low as possible. The shunt resistance in the solar cell is due to leakage across the p-n junction. The crystal defect or impurities present in the junction leads to such resistance. The desirable value should be high as possible.

A1.8 Light Trapping in Solar Cell

The primary objective of the present thesis is to fabricate a cost-effective solar cell. As the high-grade silicon material cost contributes more than 60% of the overall solar cell cost, we attempt to use less silicon material thin silicon as an absorber material. We have used commercially available 180 μm wafer as the starting material of the solar cell, by reclining the substrate to ~30 μm thickness. We have reported the benefit of a thin wafer in terms of increasing production throughput. Apart from this economical prospect, in thin Si, bulk recombination decreases, however, it raises more severe problems, i.e., increased surface recombination and partial optical absorption. High light absorption through photon management is one of the biggest challenges for realizing high efficient solar cells using a thin silicon wafer. For the effective utilization of the incident solar radiations, photon management is required to enhance the absorption. The overall

tactic is to keep incident light trapped inside the absorber layer until it gets absorbed by the materials. The primary purpose of the light trapping scheme is to increase the effective optical thickness of the wafer in comparison to the thickness of the used wafer.

Generally, there are two effective ways of light trapping. In the first approach, the average photon path length inside the thin silicon wafer or absorber layer is increased. It is accomplished with the help of light scattering by introducing a rough surface interface. This technique is popularly known as surface texturing or by forming silicon microstructure on the front surface [84-87]. When a light incident at the textured surface, the microstructure helps to prolong the light traversed path by multiple reflections, back and forth, confining the light inside the absorber layer. This integrated reflectance reduces upto 10-12% within the solar spectrum 300 nm-1100 nm *wrt* spectral photon density φ(λ). Mathematically, integrated reflectance is given as

$$R_{bi} = \frac{\int_{\lambda 1}^{\lambda 2} \phi(\lambda) R(\lambda) d\lambda}{\int_{\lambda 1}^{\lambda 2} \phi(\lambda) d\lambda} \tag{1.6}$$

where $R(\lambda)$ is the wavelength-dependent reflection, and $\phi(\lambda)$ is available spectral photon density.

The second approach would lead by light manipulation or photon propagation in the solar cell. In this technique, single or multiple optical-active layers are deposited as an anti-reflecting layer at both the front and rear sides of the cell. These layers form optical cavities, which act as back reflectors. Photonic crystals, gratings etc can be used for the back-reflection purpose [88-92]. Another innovative method for light trapping is achieved by the inclusion of dielectric or metal nanoparticles as surface plasmons, which enhanced the absorption in the solar cell [93-95]. The as-mentioned light-trapping scheme may be implemented individually or in combination with one another depending on the applications. These light trapping schemes are discussed, in detail, in the following section:

1.8.1 Texturization of silicon substrate

In 1960, *B. Dale* and his group proposed the novel method of surface texturization for silicon substrate [96]. The purpose of texturization is as follows [97]:

i. It significantly reduces the front surface reflection from 30% to 10%;

ii. Increased optical path length by following oblique trajectory;

iii. It helps in increasing the effective absorption coefficient by trapping weakly absorbed light due to encountering multiple reflections in between the front and the rear surface.

In recent years, several techniques have been adopted to acquire different textured geometries for reducing the reflection coefficient to trap more and more light into the silicon substrate [98]. There are several textured geometries (Fig.1.9) that were realized on silicon substrates at different conditions. Some of the examples are (a) micro/nanopyramid, (b) regular inverted pyramids, (c) random upward pyramid, (d) random inverted pyramid, (e) honeycomb structure, etc.

Atoms in a silicon wafer are arranged in different symmetries, i.e., faces and directions. Henceforth, the physical properties are dissimilar in different crystal planes and directions (Fig.1.10). So, for texturization, selective etching is carried out in different crystalline faces. For silicon texturization, alkali etching was performed in 20% KOH or NaOH solution at a constant temperature of 85°C. The chemical reaction governs between the silicon and alkali solution is as follows:

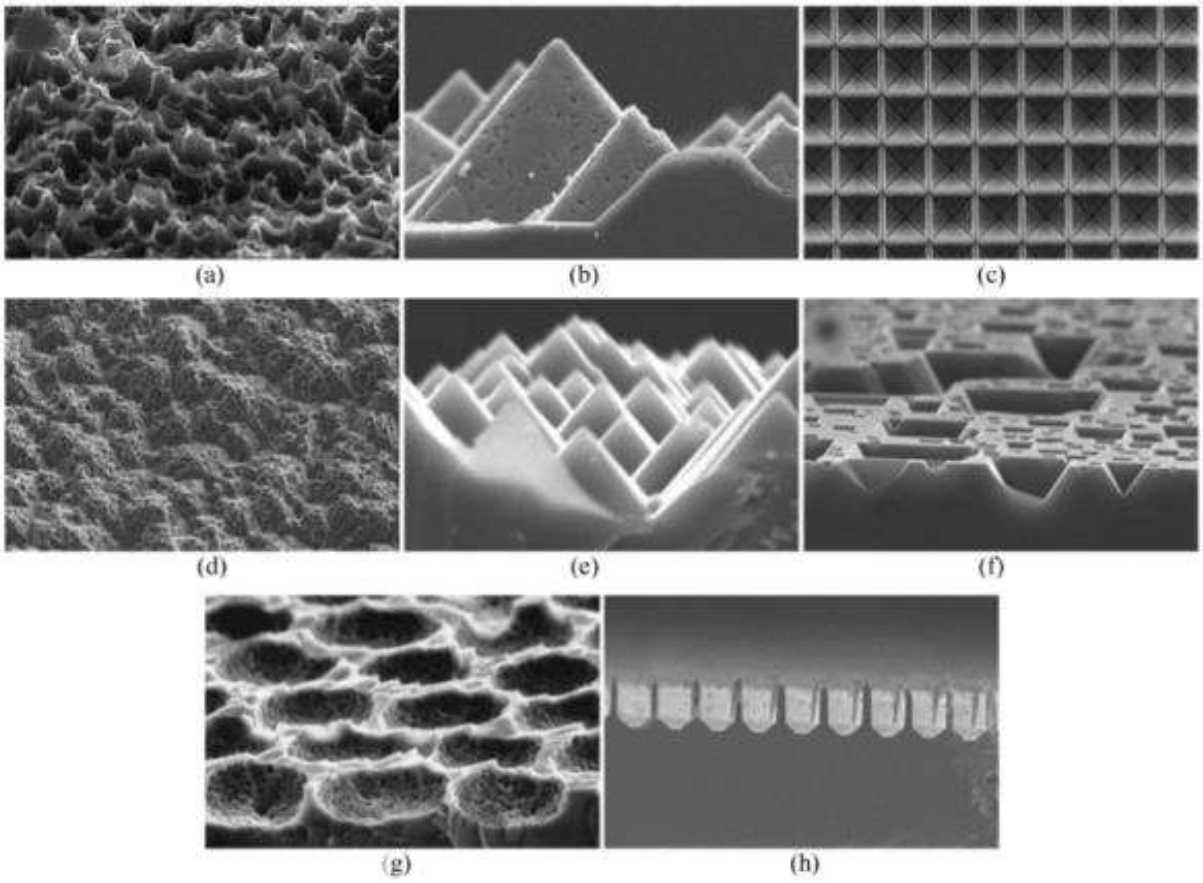

Fig.1.9: Different texturization patterns on c-Si (a)Random Conical, (b) Micro/nano pyramids, (c) Regular Inverted pyramid, (d) Porous upward pyramids, (e) Random upward pyramids, (f) Random upward pyramids, (g) Honeycomb, and (h) Grooves (Reproduce with permission of Elsevier) [98].

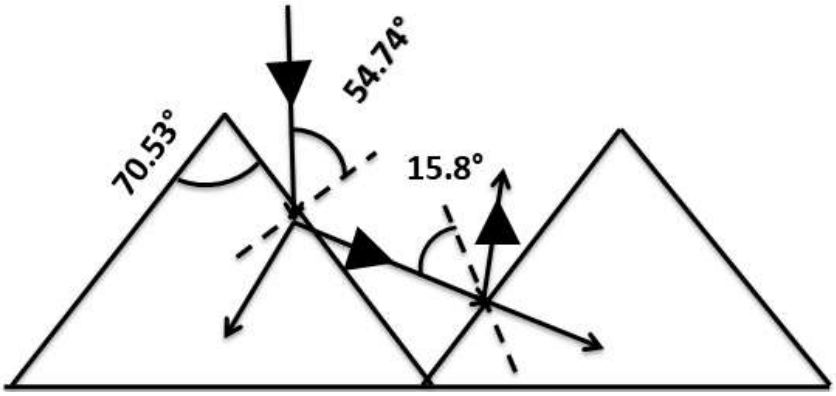

Fig.1.10 Schematic of light trapping process by textured surface in Si wafer.

$$Si + 2\,OH^- + H_2O \rightarrow SiO_3^{2-} + 2H_2 \uparrow$$ [97]

According to the electrochemical corrosion, the etching rate of the alkali solution is distinct in different planes. It depends upon the interplanar distance as well as the density of covalent bonds. For instance, the interplanar distance in (100) plane is maximum and therefore density of covalent is minimum. On the other hand, the interplanar distance is minimum in (111) plane and while covalent bond density is maximum. As a result, (100) plane is more prone to breakage, and the etching rate is minimum along the (111) plane. However, the etching rate is minimum along the <111> direction. Therefore, with the help of anisotropic and selective etching (100) plane, it is easy to exposed (111) plane. The upward pyramid form by the texturization is due to the intersection of the four (111) planes and one (100) base plane. Generally, alkali solution is used for selective etching of (100) plane. The etching rate depend upon the two processes:

i. Reaction rate at the surface

ii. Reaction rate at which reactants (alkali solution) diffuses into the surface.

These processes control the etching of the silicon wafer. Isopropyl alcohol (IPA) acts as a catalyst for increasing the rate of surface diffusion and is responsible for microstructure growth [99].

1.8.2 Black Silicon

Black silicon (BSi) refers to a silicon wafer whose surface is modified with a nano or fine microstructure layer. Such structure effectively reduces light reflection bya factor 45%. Additionally, Black silicon enhances the scattering and absorption of light, over a wide spectrum range, resulting in black perception instead of silver-grey. Black silicon possesses several interesting characteristics, such as low reflectance, good-chemical activity, large active surface area, super-hydrophobicity, and high-luminescence efficiency (considering nanopattern feature sizes are limited to a few nanometers). There are several methods reported for the simple fabrication of black silicon. Some of these

methods are reactive ion etching (RIE), metal-assisted chemical etching, electrochemical etching, strain etching, or laser etching [100]. Black silicon generally comprises a needle or wire-shaped microstructure as shown in Fig.1.11. Fig.1.11 is fabricated using the deep RIE or Bosch technique. In deep RIE, SF_6 and C_4F_8 (Octafluorocyclobutane) gases are alternatively introduced into the chamber for switching between etching and passivation, respectively. The silicon needle size is in the range of a few nanometers to several micro-meter (μm) or sometimes even more. The size of the needle depends upon the thickness of the wafer as well as the etching rate. Another etching technique i.e. Bosch RIE process uses cryogenic reactive ion etching (RIE) which incorporates alternate etching and passivation by initial sidewall passivation by oxygen gas, forming SiO_2. The subsequent removal of SiO_2 is by directional ions. Another method for realizing black Si is *Mazur's* method. In this method, the silicon wafer is exposed with a femtosecond laser pulse [101] and after exposure of high-intensity short pulses, the wafer is placed in the chamber and

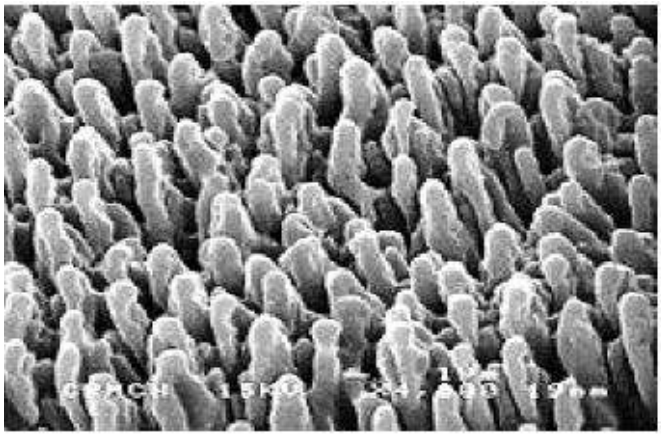

Fig.1.11: (a) SEM image of self-organized nano or micro-sized cones (Reproduce with permission of Elsevier) [102].

sulphur hexafluoride (SF_6) followed by passing ofother dopants through the same wafer. Fig.1.11(a) shows the SEM image of self-organized nano or micro-sized cones [102]. Penguin structure is also realized by this method, however, in a gas environment using a non-reactive chamber Fig.1.11 (b)). Scanning Electron Microscopy (SEM) images of

such wafers showed that microstructures became blunt in comparison with the structure developed in the presence of SF_6. Both the structures induce less reflectance over a broad area of the solar spectrum.

1.8.3 Nanopores

Metal-assisted chemical etching is a popular method for fabricating nano-pores to reduce reflection from the top surface. First, we deposit the thin layer of metal nanoparticles such as copper (Cu) or silver (Ag) on the silicon wafer for realizing nano-scale pores. These metal nanoparticles withdrew electrons from the silicon wafer and oxidized the surface. Later on, it is treated with hydrofluoric acid (HF) to etch down the oxidized surface and forms an inverted pyramid shape such as nano-pores into the silicon. Fig.1.2(a) shows the texture and cross-sectional SEM image of the Cu-assisted chemically-etched Si surface, whereas Fig.1.12(b) shows the inverted pyramid structure [103].

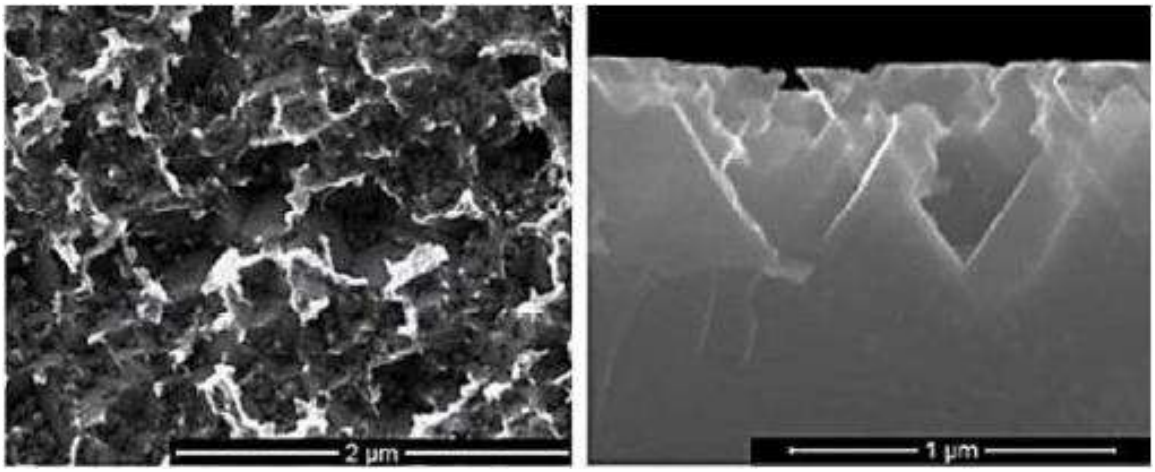

Fig.1.12: (a) SEM image of a top surface (b) cross-section of a Cu- assisted chemical etched silicon surface (Reproduce with permission of journal of Materials Chemistry A) [103].

1.8.4 Antireflection coating

Antireflection coating (ARC) is a thin layer of dielectric material, which is generally deposited on the top surface of solar cells to reduce the reflection of incident light by a destructive interference process. The thickness (d) and refractive index (n) of

the layer are wisely chosen to fulfill the harmful interference conditions to achieve the best anti-reflection properties. The thickness (d) of the dielectric layer needs to be chosen in such ways that there must be a phase difference of 180° between the radiation reflected from the air-ARC interface and the ARC-semiconductor interface. This further causes destructive interference resulting in minimum or nearly zero reflectance from the as-prepared Si wafers. In general, the thickness of the ARC should be a quarter of the solar spectrum wavelength.

$$d = \frac{\lambda_0/n_1}{4} \tag{1.7}$$

where λ_0 corresponds to the wavelength of incident radiation in air and λ_0/n_1 corresponds to the wavelength of radiation in a dielectric medium having $n_1$refractive index. According to equation 1.7, the antireflection coating will show minimum reflection only at a particular wavelength and for other wavelengths, the condition of destructive interference will not be true. A wise selection of ARC thickness will yield minimum reflection in the solar spectrum.

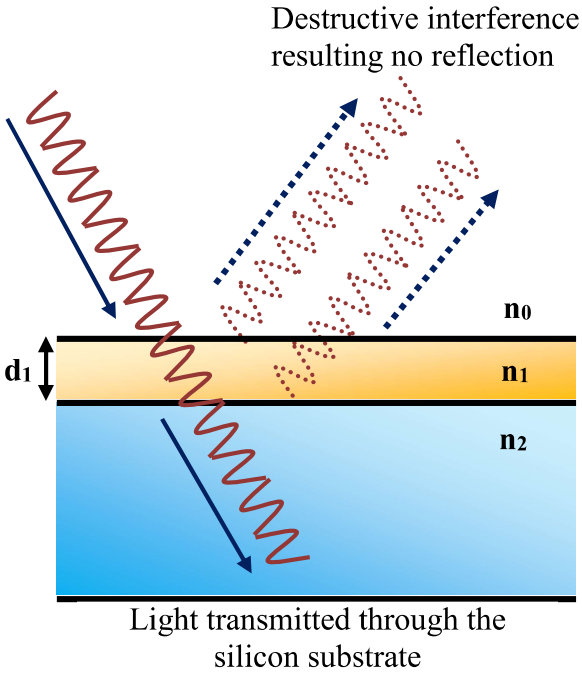

Fig.1.13: Schematic of destructive interference caused by antireflection coating.

Generally, solar panels are encapsulated in the glass substrate, which affects reflection from the ARC-semiconductor interface and changes the value n_1, which is important for the overall process to achieve minimum reflection. Mathematically, minimum reflection R_{min} given in terms of n_0, n_1, and n_2 as shown in the equation 1.8:

$$R_{min} = \left(\frac{n_1^2 - n_0 n_2}{n_1^2 + n_0 n_2}\right)^2 \quad (1.8)$$

Whereas n_0, n_1 andn_2, represents the refractive index of air, antireflecting coating, and silicon respectively. For minimum reflection the following condition needs to full-fill:

$$n_1 = \sqrt{n_0 n_2} \quad (1.9)$$

At present, in the industry flow-line, a ~80-90 nm thick silicon nitride Si_3N_4 (having a refractive index(n_1 ~1.9)) is used for commercially viable ARC.

1.8.5 NanoparticleassistedLight scattering

One of the effective mechanisms for light trapping is to increase the absorption using the resonant surface plasmon effect created by nanoparticles (NP). In the resonant surface Plasmon effect, the incoming electromagnetic field and free electron on the dielectric or metal nanoparticles' surface interact. The interaction process offers a large field near the surface where the light absorption and the trapping increase in the cell. The detrimental effects (transmission loss etc.) of a thin (~30 μm) silicon wafer are the fundamental limitation for its practical application. At present, all the commercial solar cells are fabricated on optical thick (180-300 μm) wafer owing to these limitations. However, in the thick wafer, the generated charge carriers are too much away from the junction, and these charges are unable to sweep out by the junction's built-in potential. Consequently, charges are recombined due to the effect of the bulk recombination process. The limitation of a thin wafer may conquer some limits by incorporating nanoparticles of optimized diameter and distribution. The limitation of the thin wafer may

conquer up to some limit by incorporating nanoparticles of optimized diameter and distribution. The inclusion of nanoparticles increases the optical path length leading to the generation of charge carriers and short-circuits current [100]. Generally, the plasmonic effect increased the conversion efficiency of the cell by three methods. In one method, the nanoparticles induce sub-wavelength scattering enhancing the light trapping by increasing the optical path length. In another approach, the nanoparticle, present at the top of the active material, may be treated as sub-wavelength antennas and coupled the light into the guided mode, thereby increased the absorption into the active or semiconductor material. The third approach includes incorporating back patterned metal contact, which helps to couple higher wavelength light into the guided modes. It also helps keep the surface plasmon polarization modes (SPP) supported by the back semiconductor/metal interface. Generally, there are four types of light trapping phenomenon as shown in Fig.1.14 exerted by the metal and dielectric nanoparticles. A brief discussion on the process is given below.

1.8.5.i Light trapping by metal nanoparticles

Metal nanoparticles having a sub-wavelength dimension enhanced the light trapping event. It couples the light into active material due to multiple and high-angle scattering, which increases the optical path length in the absorbing material. Further, the elongated path length helps light to absorb and enhance the photon injection in the junction. This technique is reported more useful comparison to the use of the NP layer at the top. After the device processing, it works on a broad wavelength range.

1.8.5.ii Light trappings by metal nano-antennas

Metal nanoparticles or nanostructures with appropriate dimensions are used as plasmons-based light concentrators, enhancing the light trapping in an active material called a sub-wavelength antenna. When light falls on these nanostructures and NP layer,

the plasmonic near-field is coupled with them increasing the effective absorption cross-section of active absorbing material that is immediate to nanostructure. This plasmonic near-field enhances the light absorption and generates an electron-hole (e-h) pair in the absorbing medium. This type of structure works well only for small metallic nanoparticles (5-20 nm), for which the scattering cross-section is less than the sum of scattering and absorption. This technique is helpful for materials having a small carrier diffusion length. In the presence of metallic nano-antenna, the efficient energy conversion occurs when the absorption rate of the absorbing material must be greater than the reciprocal of typical Plasmon decay time (10-50 fs.) otherwise absorbed energy dissipated as ohmic damping into the material [105].

1.8.5.iii Enhanced surface Plasmon polariton coupling by metal nanostructure

The coupling of surface Plasmon polariton (SPP) with metal nanostructure is only beneficial when absorption by SPP in the semiconductor is much larger than the metal nanoparticles. Here, light is first converted into the SPP by metal nanostructure; after that, light passes through the metal/semiconductor interface and is confined due to the plasmonic resonance frequency. It is applicable for structures having a dimension smaller than the incident light wavelength. In the presence of adequate optical engineering, we can easily couple more photons into the active or absorbing medium. This technique may be coupled with the conventional metallization process for a better solar cell prospect, especially in silicon solar cells [106-108].

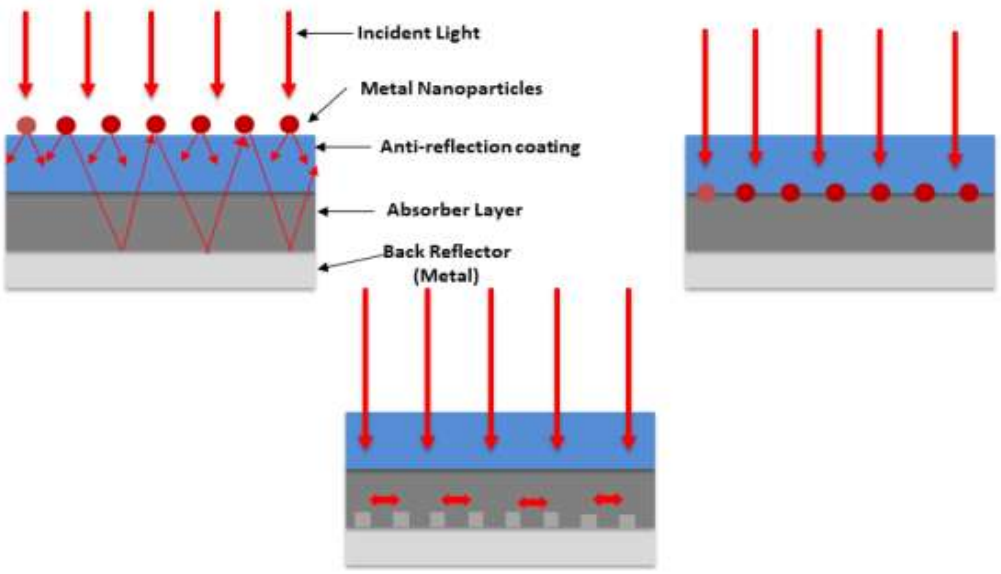

Fig.1.14: Different light trapping schemes using dielectric nanostructure: (i) light scattering with the help of plasmonic nanoparticles (ii) light trapping with the help of nano-antennas and (iii) photon generation with the help of surface Plasmon resonance mode.

A.1.9: Plasmonic light trapping: Metals or dielectric?

There are several inherent disadvantages of incorporating metal nanoparticles in the solar cell because metal nanoparticle surfaces may act as a recombination centre and subsequently reduce the cell's efficiency. The scattering and absorption resonance frequencies of metal nanoparticles are almost the same, which results in *Joule heating loss*. The way to mitigate this effect is by incorporating transparent conductive oxide (TCO) or dielectric nanoparticles in the cell. Dielectric nanoparticles exhibit low absorption and high scattering efficiencies, which make them suitable candidates to couple more photons into the junction or active material with minimal self-absorption (due to high bandgap value) [108,109]. As dielectrics are generally insulating in nature, hence passivation in the device is unaffected. Due to the lossless behavior of these dielectrics, it also restricts the temperature of the device and results in high V_{oc} as well. So, due to these excellent properties of the dielectric nanoparticles, these are the

outstanding candidates for both thick and thin c-Si solar cells to improve efficiency at the top as well as the rear surface of the cell [110-112].

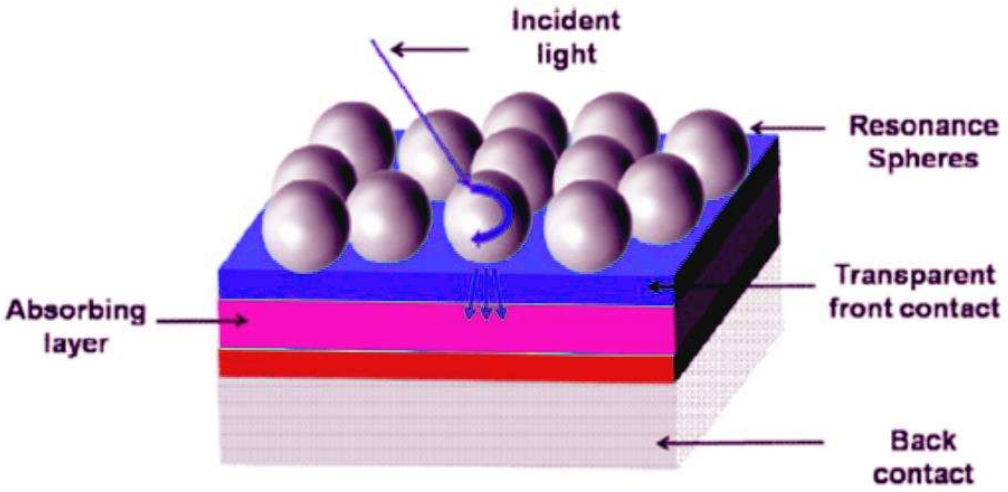

Fig.1.15: Schematic representation of light trapping into the absorber layer through the dielectric resonating sphere.

Dielectric NP has a unique property of forming whispering gallery modes (WGM) into the particles, and Rayleigh first observed this in 1878 [113]. This phenomenon was first reported for acoustic waves in big size dome structures (Fig.1.16). After that, various investigations say that such phenomenon also exists in Electromagnetic waves: i.e., in radiowaves, terahertz- radiations, microwaves, infrared radiations, and X-rays. Here, in the dielectric sphere *total internal reflection* (TIR) is pronounced due to the inner surface of the sphere-like structure. Some particular diffraction modes of the electromagnetic wave travel along the periphery of that shape wall get trapped into it.The quality factor (Q), of such structure, is a crucial factor that affects the losses and resonating frequency. In a dielectric sphere, when light falls, electrons start resonating at different frequencies, increasing the absorption of a wide range of wavelengths of light. Further, it helps to trap WGMs and guide the high refractive index absorber layer (like silicon) due to the refraction grating at the interface. The appropriate dimension and distribution of the dielectric material may ensure maximum photon injection into the silicon substrate. This is why the modern age research community focuses on the dielectric lossless nanospheres

as an antireflection coating on silicon solar cells. Some recent studies confirm that the dielectric nanospheres employ *Mie resonances* to store and couple the light virtually into the silicon substrate [114]. This phenomenon also largely depends on the geometrical cross-section and the cavity quality factor of the particle. Furthermore, the utilization of dielectric spheres as nano or microlenses to inject the maximum photon into the junction of a solar cell is also very common nowadays.

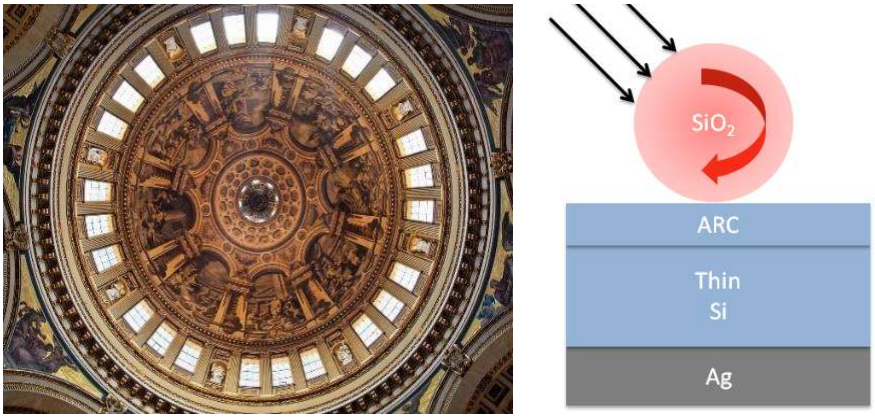

Fig.1.16 (a) St. Paul's cathedral, London, England where the WGM mode was noticed first by Rayleigh [115]; (b) Enhancement of light trapping into the thin Si solar cell using dielectric sphere through WGM modes.

For better light management, the optimization of the focal length is required, which can be executed by tuning the particle's size and shape. Such evidence is well studied globally and established by different research groups, which indicate the effectiveness of dielectric particles to realize high efficiency or thin c-Si solar cell [116].

A 1.10: Future roadmap for the realization of High-efficiency solar cell

The fabrication of affordable, highly efficient solar cells is a tiresome process, and several targets are yet to achieve. For the systematic fabrication of such a sophisticated solar cell device, the following key points should well be taken care of, as given in Fig.1.17. A highly efficient solar cell can be developed by minimizing the significant losses by following the steps mentioned earlier. These losses are photon loss, carrier loss,

and electrical loss, which are well-reported and explored. However, the future solar cell technology does not always intend

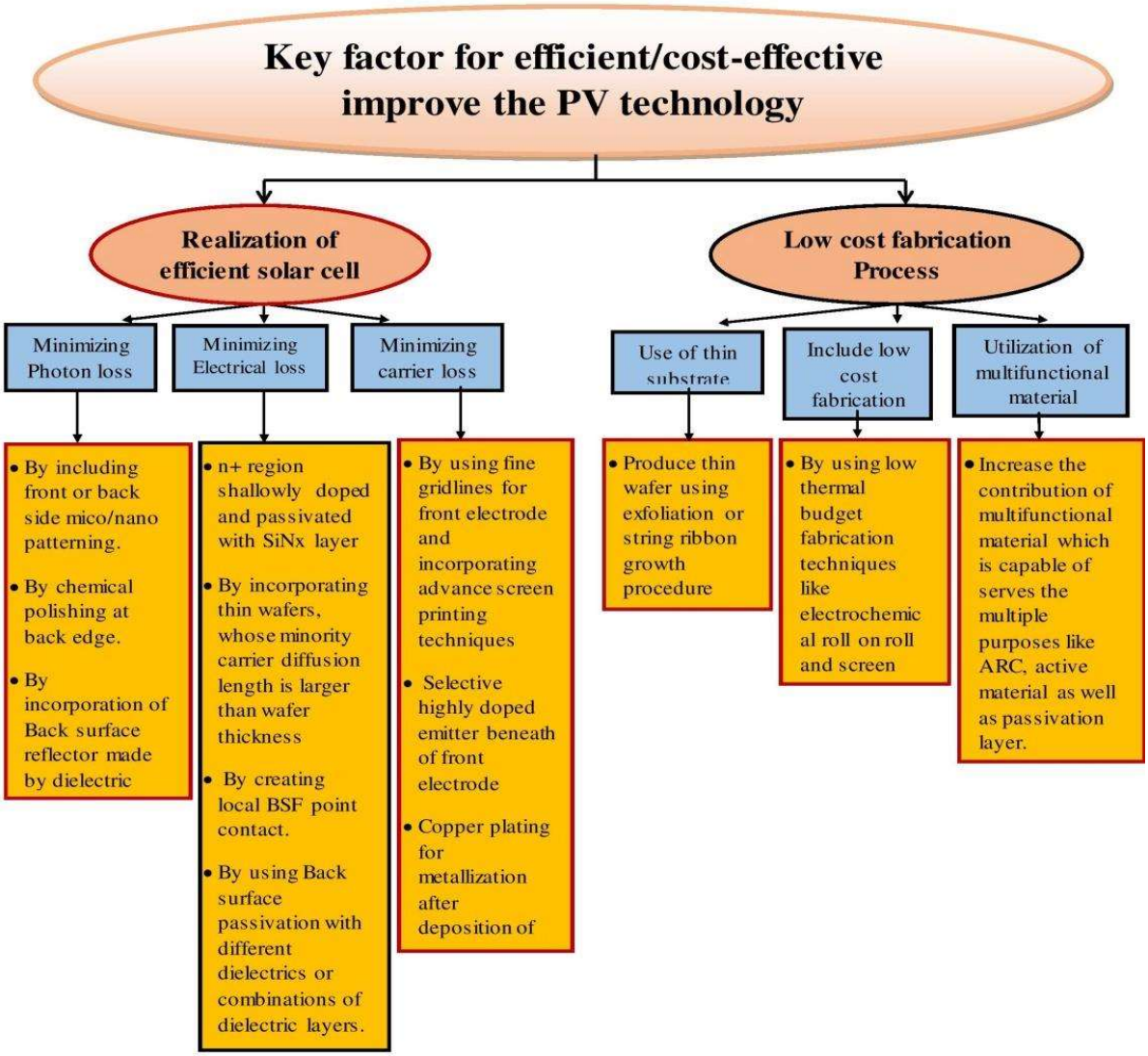

Fig.1.17 Key factors for the development of efficient and affordable PV technology.

for its efficiency; instead, the cost-effectiveness, flexibility of the structure, and compatibility with future electronics are also serious challenges that need to be considered simultaneously. To achieve above mentioned challenges thin (~10 to 30 μm) wafers is required to fabricate the solar cell. These are cost-effective due to the use of lesser material and additional features like flexibility. Such thin wafers can be processed by using the laser cutting technique; however, laser-material processing is yet to develop to

achieve precision. Generally, for fabricating solar cells, chemical etching is used to make thin wafers (~30μm). On the other hand, c-Si, instead of different materials like organic, perovskite, dyes, and metal oxides, provide the additional advantage of stability. The main points of *cost-effective approaches* have been elaborated in the following sections.

A1.10.1 Use of thin c-Si wafer as substrate material

It is well known that most of the commercially available solar cells are fabricated by using 180-220 μm thick c-Si wafers. The net solar cell's net cost is due to its material cost which is approximated more than 50% of its cost. Schockley-Quiseer has mathematically proved that the ~30 μm thin c-Si solar is suitable to produce a high-efficiency solar cell. Thus, the costs of the solar cell can be reduced by incorporating a comparatively thin c-Si wafer for realizing solar cells. In 1997,*Wallace et.al* proposed a method of *String Ribbon* to prepare 100 μm thin c-Si wafer directly from the melt [117,118]. It is also demonstrated in a theoretical calculation by the PC1D software, revealing the itself-potential conversion efficiency ~16%. Recently, researchers have suggested developing flexible silicon substrates having a thickness of 50-70 μm using the explorations technique. The measured lifetime of such wafer is around 120 μs. Realizing a large-size thin wafer by this technique is quite complicated [119]. Especially the uniformity of the wafer is a challenging issue. The wafer's non-uniformity affects the surface passivation. In 2005, Lee *et.al* proposed the *Transfer Printing* technique for the production of the thin c-Si solar cell. Researchers have successfully reported thin and flexible c-Si solar cells fabrication using chemically etched substrate in the current scenario. This chemically-etched thin c-Si wafer is not suitable for industrialization due to the high material wastages. However, making prototype fabrication assumes the efficiency and usefulness of thin silicon-based flexible solar cells. This further encourages researchers and industries to develop thin/ultrathin c-Si substrates in mass quantity using

a loss-less approach like laser cutting. Fig.1.8 demonstrates a thin ~30 μm and flexible c-Si wafer produced as a part of this present work.

Fig.1.18: The developed ~30 μm thin flexible c-Si wafer by alkali etching during the research work.

A 1.10.2 Building up fabrication techniques

As we know, in the photovoltaic industry, cost and efficiency both are essential factors. If we want to improve the fabrication process and bring down the device's cost, then the low-thermal budget technique should be included in the production chain. The low-budget fabrication process like screen printing, electrochemical depositions are well accepted by the research community. Similarly, sophisticated technologies, including high-vacuumed devices (like diffusion furnaces, PECVD, sputtering units, etc.), are introduced in the fabrication process to reduce the thermal budget.

A 1.11 Conclusion and Scope of the work

In the present work, we have surveyed the literature; shed light on current trends in PV technology,and a brief review on the chronological growth of technology. As a result, we concluded at least two major vital issues, which need to address for the successful implementation of solar photovoltaics as a clean energy source across the

globe. These issues are efficient and low-cost solar cells. The silicon technology and fabrication techniques have witnessed enormous growth and left little scope for further cost reduction. The possibility of reducing the cost of the solar cell is by cutting down its material cost. It is shorted out by incorporating a thin c-Si wafer for the fabrication of solar cells. As described in the previous section *1.6.1.1,* efficiency depends upon the absorbing material's thickness, so light-trapping strategies must be incorporated to achieve the efficiency comparable to the conventional solar cell. The conventional thick wafer ~180 μm may replace from the industrial production line by incorporating a thin c-Si wafer (~30 μm) and various issues of thin solar cell like low light trapping mechanism can be avoided by incorporating proper light trapping techniques, especially at the bottom of the c-Si solar cell. This thin wafer gives an additional benefit in terms of flexibility, by which the c-Si solar cell can be easily incorporated with roll-to-roll electronics. This thin c-Si wafer (~30μm) does not affect electrical properties or electrical losses too much but increases the optical losses. Advanced light trapping schemes such as nano-patterning or plasmonics need to be incorporated to reduce such losses. In this work, we fabricated prototype c-Si solar cells on a thin (~30 μm) c-Si wafer as a pilot scheme,and proper measures were taken to address the light trapping issues in thin c-Si substrates without compromising with the electrical properties of the device.

Part-B: Experimental and Characterization techniques

In previous sections, we discussed the fundamental of the c-Si solar cell, light trapping mechanisms, and various designing criteria for better absorption of light in a solar cell to make solar PV efficient and cost-effective. Although various materials are reported other than silicon with their exceptional performance, mono-crystalline silicon wafers are still preferred by photovoltaic industries due to their better stability, good module efficiency, etc. In this work, a ~30 μm mono-crystal p-Silicon wafer was used as the starting material for fabricating a single-junction solar cell, silicon heterojunction, and organic-inorganic solar cell. In the following section, we will discuss the different types of techniques associated with the fabrication of silicon solar cells. Further, different solarcellcharacterization methods arealso discussed in the following sectionsfor a detailed understanding of the properties and device performance.

B1.1 Wafer Preparation

1.1.1 Saw- Damage removal and thinning of the wafer

Initially, the as-cut wafer's surface was rough and polishing and lapping were performed to improve the surface structure. KOH and NaOH were used via wet chemical polishing to remove the saw damages in the wafer. This is a promising and conventional method to reduce the reflection loss. Further, it uses to convert thick (180 μm) c-Si wafer into thin (~30 μm).Furthermore, the wafer is dipped into the 10% Sodium hydroxide (NaOH, 97%) at 80°C for 80 minutes to remove the saw-damage and thin out the as-cut c-Si wafer [120]. The etching rate of the c-Si wafer is around ~1.8 μm per minute.

1.1.2 Cleaning

Cleaning is an essential step for the fabrication of solar cells. Without proper cleaning of the wafer, the device will unable to give its optimum performance. Metal

particles present on the wafer's surface affect the passivation, minority carrier lifetime, and efficiency of the cell. The presence of organic, oxides, etc., degrades the junction's quality, affecting the charge carrier separation. One of the most successful and popular cleaning techniques used in the semiconductor industry is *Radio Corporation of America* (RCA) standard cleaning [121]. The RCA cleaning process comprises of two steps. *Standard clean-1* (SC-1) and *standard clean-2*(SC-2). The purpose of incorporating SC-1 is to break down the organic molecule and complexes of Group I(B) and II(B) metals and other metals like Au, Ag, Cu, Ni, Zn, Cd, Co, and Cr. In this process, ammonium hydroxide (NH_4OH, 30%), hydrogen peroxide (H_2O_2, 30%), and water (H_2O) were taken in the ratio of 1:1:5. The SC-1 solution slowly dissolves the thin native oxide layer on silicon and continuously grows a new oxide layer by *oxidation* technique. This combination of etching and reoxidation helps to dislodge particles from the wafer surface. Recently, megasonic vibration is incorporated along with the SC-1 cleaning technique, to remove organic contaminants mechanically. After that, the oxide film grown is etched in a low concentration (1:100) of aqueous Hydrofluoric acid (HF, 49%) solution. In the next step of cleaning i.e. SC-2, the wafer is dipped into a mixture of Hydrochloric acid (HCl, 37%), Hydrogen peroxide (H_2O_2, 30%), and water in the ratio 1:1:6 by volume, and heated at 70°C for 10 minutes. By incorporation of SC-2 the remaining metal impurities have been completely removed, which didn't remove by SC-1 process.

1.1.3 Texturization

Absorption of light is significantly reduced in thin wafers. Hence, a light-trapping scheme is essential for the fabrication of thin wafer solar cells. In a thin c-Si cell, the physical thickness of the absorber layer is thin. Further, to compensate for the physical thickness, we have maximized the wafer's optical thickness by increasing the incident photon's optical path length. Isotropic etching of Si (100) in KOH & isopropyl alcohol

(IPA) solution was used for texturization, a well-established technique. In which a wafer is dipped into this solution and maintained at a temperature of 80°C [97,98]. Due to this process randomly distributed pyramids were observed and these pyramids were developed, since, the KOH selectively etch Si (100) over (111) planes [99].The size of the pyramid and its distribution depends on the initial wafer surface, solution process temp, and concentration.

B1.2 Deposition techniques

1.2.1 Sputtering

A sputtering technique can deposit a high-quality film due to the availability of high purity gases and vacuum of the order ~10^{-7}(mbar). In this technique, the chamber is filled with inert *argon(Ar)* gas at low pressure, and plasma is generated between source/target material and material after applying the voltage. The plasma (high energy argon ions) etched the source material atoms from the target and condensed (deposited) on the substrate. Radio frequency (RF) and direct current (DC) sputtering are commonly used for the deposition of metals and insulators. DC sputtering is unable to use for insulators because due to accumulation of charge at the source electrode weakens the voltage required to maintain the plasma required for sputtering deposition. The semiconductor film is deposited using the compound source target or by the other reactive sputtering method. Today, the advanced co-sputtering machine is also available with multiple targets, facilitating the growth of multi-stacking of films without breaking the vacuum.Films of nm to several micrometers thickness can also be prepared by using the sputtering technique. Generally, the sputtering system consists of rotary and the turbopumps to achieve a base pressure of 10^{-6} mbar. As such system is capable to work in RF as well as in DC mode. At RF 13.56 MHz frequency is used. Argon is used for

generating the plasma. A substrate heater is also provided which heatsthe material upto 300°C.

1.2.2 Plasma enhanced chemical vapour deposition

For the fabrication of silicon heterojunction solar cell (SHJ), Plasma enhanced chemical vapour deposition (PECVD) technique is used for deposition of i-a-Si:H and doped (p & n) type layers. This deposition was carried out with the commercially available PECVD deposition system (Hind High Vacuum Ltd. (HHV), India). This deposition system has four chambers with one common central loading/unloading chamber, as shown in Fig.1.18, and all the chambers are connected by a pumping scheme as depicted in Fig.1.19.

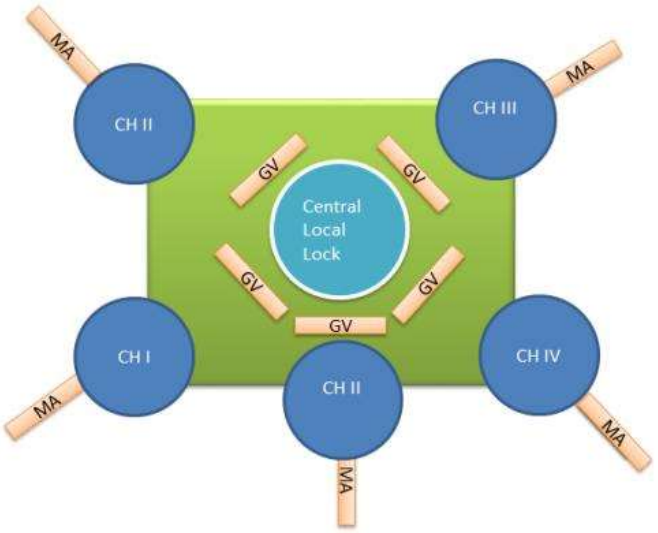

Fig.1.19(a): Four chamber PECVD cluster tool (CT-150) with load lock.

The reactive gas flows in the chambers werecontrolled by using mass flow controllers (MFCs), and these reactive gases when reacts to each other or decomposes and the final materials deposited on the substrate. Before deposition, the chamber vacuum was kept at 1.33x 10^{-7} mbar by using turbo-molecular pumps. The reactor chamber is made of high-grade stainless steel containing two stainless parallel electrodes in a diode configuration. These two electrodes are flatbed type, symmetrical, and internally capacitive coupled.

Fig.1.19 shows the schematic representation of the electrode assemblies where the cathode is connected with a power supply through an impedance matching (L-C) network. During the deposition substrate holder acts as anode and the chamber wall acts as ground. The lower electrode is also grounded to confine the plasma between the electrodes and avoid deposition on the chamber's inside of the wall. All the parameters such as gas flow, chamber pressure, RF power, the substrate temperature are controlled through a programmable logic circuit (PLC) using the full name SCADA (supervisory control and data acquisition system). The electrode which is connected to the deposition system has afixed diameter of 15 cm. The power can be varied from 0-300 watt as per requirement or optimized for deposition. Semiconductor grade gases are used in the deposition chamber and its flow is controlled by MFCs through the lower electrode in a spray

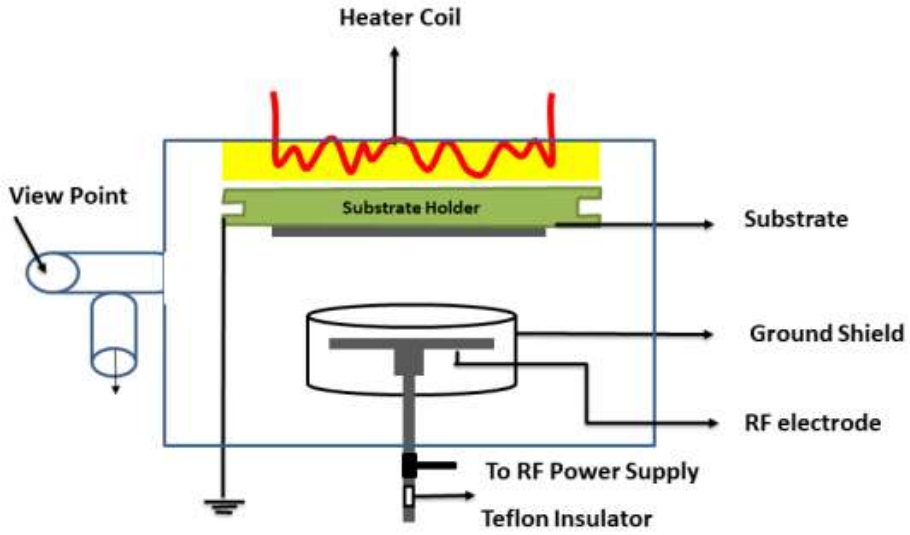

Fig.1.19(b): Gas supply, pumping and other parts of the PECVD cluster tool.

type way. The chamber pressure is controlled by the butterfly valve which is attached to the gas exit line previous to the oil rotatory pump and capacitance manometers (Inficon, USA). The separation between the electrodes was 20 mm and always fixed [123]. The composition of the gases and recipe used for the fabrication is provided in the respective chapter where they have appeared.

1.2.3 Metallization

In a conventional c-Si solar cell, the screen printing technique is used for making the contacts, but this technique cannot be used for making contacts in a thin c-Si solar cell due to the less mechanical stability of the thin c-Si wafer. Instead of using the conventional method for making contact through screen printing, the thermal evaporation unit was used to make contacts. It was anticipated that the thin c-Si wafer might be damaged by the pressure applied during screen printing. These damage risks could be avoided via thethermal evaporation technique.

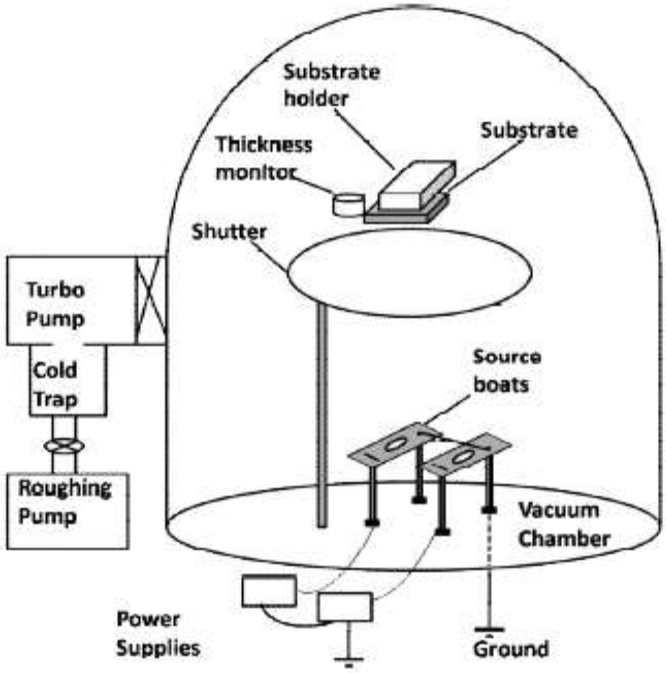

Fig.1.20: Schematic of thermal evaporation system.

It is a reliable and straightforward method for the uniform deposition of metal films. As shown in Fig.1.20, samples were mounted on a sample holder connected with a rotating disc inside the deposition chamber. The holder is mounted on the top of the tungsten boat. The source material is heated either by resistive heating or by the electron beam. Before starting the deposition of metal contacts on the sample, the chamber pressure was

maintained around 5×10^{-6}mbar. The melted source material travels through the vacuum chamber and is deposited on the substrate and the walls of the chamber. The thickness of the deposited metal layer is monitored by a quartz crystal-based digital thickness monitor. The system consists of a dry rotary pump backed by a diffusion pump to achieve pressure in the range of 10^{-5} or 10^{-6}mbar. Often, for better contact and performance of the device, post-annealing is also performed.

B1.3 Characterization Techniques

Several characterization techniques are used for testing the fabricated device as shown in Fig.1.21. The experimental details of the methods are put together in this chapter. In the process of cell fabrication, required characterization has been done at every individual step, and the corresponding details have been mentioned in the required chapters. Here, a briefintroduction regarding various characterization techniques is being discussed.

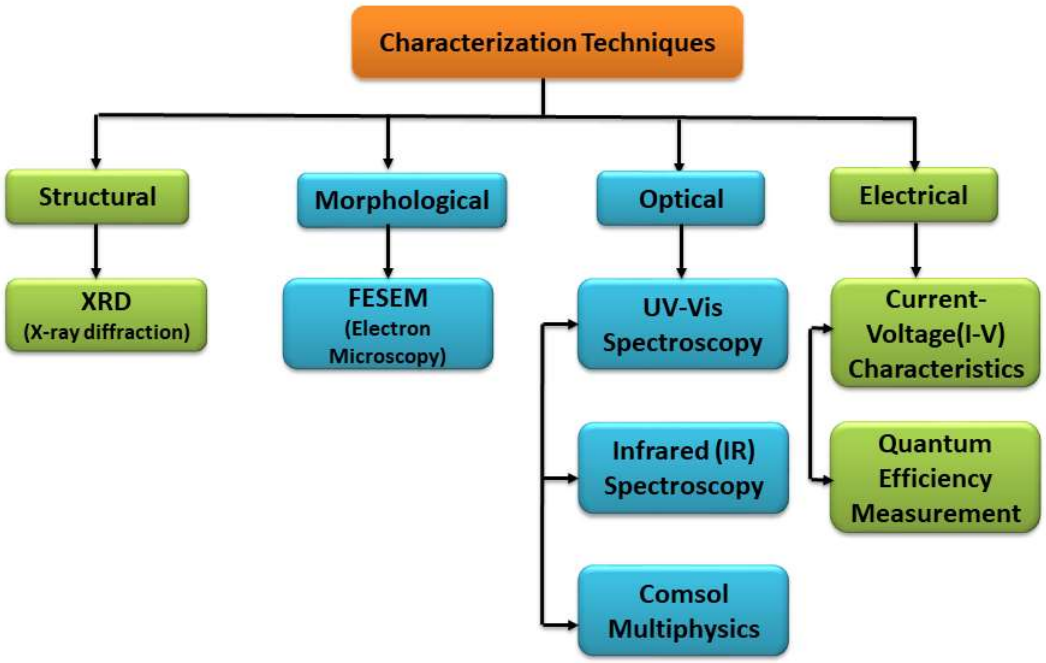

Fig.1.21: Flow chart of the performed characterization techniques for fabricated device.

1.3.1 X-ray diffraction

The concept of the X-ray diffraction (XRD) from the crystals and their analysis lies in Bragg's law:

$$2d \sin\theta = n\lambda \quad (1.10)$$

where, ' d' is the separation between the two consecutiveplanes in the crystal, 'λ' is the wavelength of the incident x-ray radiation and n 'is an integer. The powder X-ray diffraction method is ideally suited for the characterization of polycrystalline phases and powder samples.

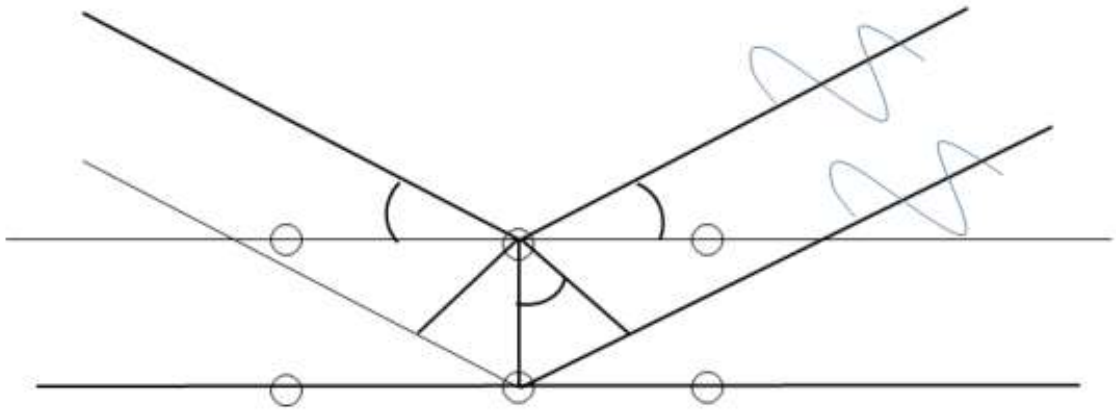

Fig.1.22: Diffraction of X-ray from the crystalline planes.

An electron resembles as alternating electromagnetic field and oscillates with the frequency of the field in all possible directions. The diffracted beams get interfere which is usually destructive. The atoms in a crystal are arranged periodically and regularly in nature, and only in a few directions constructive interference took place. When the wave is inphase, there will be well-defined X-ray beams leaving the sample at various directions. A diffracted beam consists of a large number of scattered raysthatare mutually reinforcing one another. Lattice planes inclined at small angles to the incident beam are bent about several axes, in such a manner that their planes are confined to a small cone in the space. Resulting the diffraction pattern broadened, due to Bragg's law (diffraction

condition) for the same set of planes lying on the curvature will be satisfied more than once depending on the angle of incidence with respect to the normal to the surface under condition. Moreover, the periodicity of such curvatures would eventually lead to the splitting of XRD peaks that are characteristic of the crystallographic plane of the materials. In such investigations, the X-ray diffraction measurement of the films was carried out using a Bruker D8 Advanced parallel beam X-ray diffractometer with conventional Bragg- Brentano goniometer geometry with a θ-2θ scanning mechanism. The X-ray tube is stationary and the sample moves by the angle θ. At the same time, the detectors move by the 2θ angle as shown in Fig.1.24. The peak position (2θ or 'd'values) of the XRD patterns, obtained for a particular film, were matched with the standard JCPDS database corresponding to the material, to find out the crystallographic nature of the deposited film.

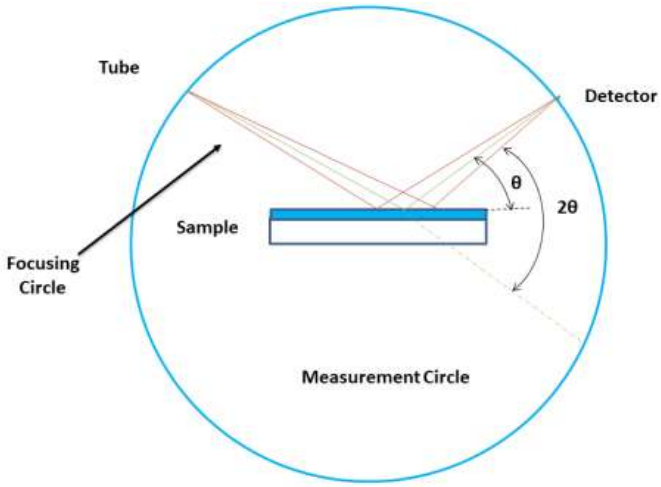

Fig.1.23: Schematic of Bragg- Brentano goniometer.

1.3.2 Surface Morphology by FESEM (field emission scanning electron microscope)

Scanning electron microscope (SEM) is an important tool for microscopic feature measurement and surface topography study. An electron microscope produces an electron beam in an evacuated column (less than $1x10^{-9}$ Pa). The vacuum allows electron

movement along the column without scattering and helps prevent discharges inside the instrument. The vacuum design is a function of the electron source due to its influence on the cathode emitter lifetime. The function of the electron gun is to provide a large and stable current in a small beam. There are two classes of emission source: thermionic emitter and field emitter. Thermionic Emitters use electrical current to heat a filament; the two most common materials used for filaments are tungsten (W) and lanthanum hexaboride (LaB_6). Thermionic sources have relatively low brightness, evaporation of cathode material, and thermal drift during operation. As a result, getting high magnification images (×100000) often becomes difficult. Field emission is one way of generating electrons that avoids these problems. A field emission source (FES); also called a cold cathode field emitter, does not heat the filament. The emission is achieved by placing the filament in a huge electrical potential gradient. The FES is usually a wire of tungsten (W) fashioned into a sharp point. The significance of the small tip radius (~100 nm) is that an electric field can be concentrated to an extreme level, becoming so big that the work function of the material is lowered, and electrons can leave the cathode. FESEM uses a Field Emission source producing a cleaner image, less electrostatic distortions, and spatial resolution < 2nm. An electron-collecting device collects these secondary electrons to produce an electronic signal. The electronic signal is amplified, and the image of the sample surface is finally displayed on the screen of a PC. Fig.1.22 schematically illustrates the essential parts of the operation of FESEM. In the present investigation, the films' surface morphologies were investigated by a field-effect scanning electron microscope (FESEM) of model ZEISS SIGMA 02-87.

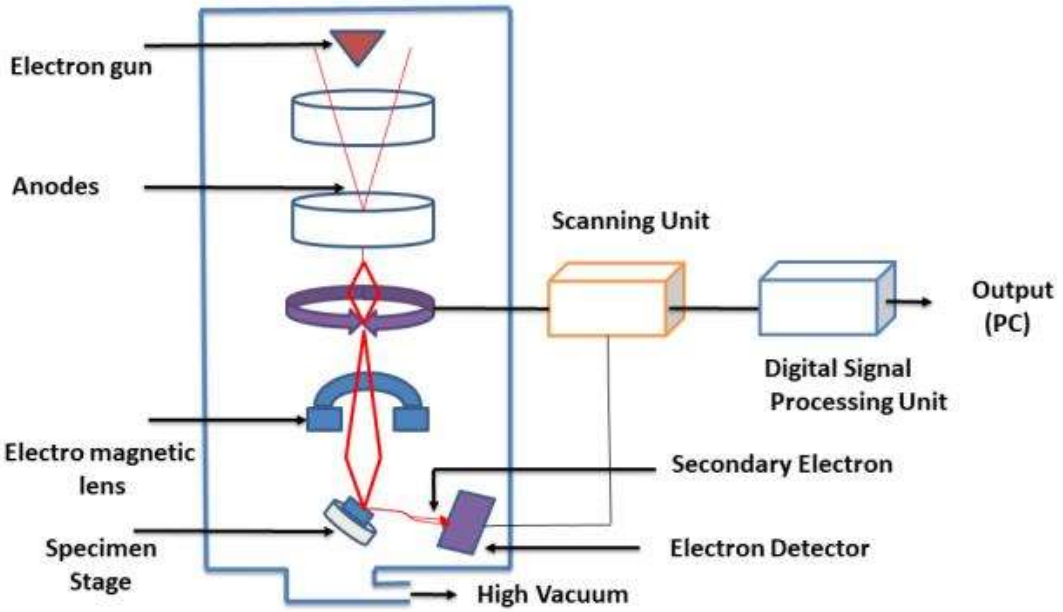

Fig.1.24: Schematic of basic operation of FESEM

B 1.3.3 Optical characteristics

1.3.3.1 Reflectance Measurement

The absorption, reflection, and transmission depend on the wavelength, polarization, and geometric distribution of the incident radiation. The reflectance R is defined by the ratio of reflected radiant power to incident radiant power. For a certain area element dA of the reflecting surface, the (differential) incident radiant power is given by the surface's irradiance E_e, multiplied by the size of the surface element, thus

$$d\Phi_{e,incident} = E_e dA \tag{1.11}$$

And the (differential) reflected power is given by the exitance M_e, multiplied with the size of the surface element:

$$d\Phi_{e,reflected} = M_e dA \tag{1.12}$$

Thus,

$$R = \frac{d\Phi_{e,reflected}}{d\Phi_{e,incident}} = \frac{M_e dA}{E_e dA} = \frac{M_e}{E_e} \tag{1.13}$$

Total reflectance is further subdivided into regular reflectance R_r and diffuse reflectance R_d, given by the ratios of diffusely (or specular) reflected radiant power and diffusely reflected incident radiant power. From this definition, it is evidentthat

$$R = R_r + R_d \tag{1.14}$$

Reducing reflectance and injecting maximum photons into the junction is the first and foremost criterion for an efficient solar cell. For this reason, a large portion of this work deals with advanced light management techniques. The minimum reflectance criteria are explained by equation1.8.

1.3.3.2 Transmittance Measurement

The transmittance T of a medium is defined by the ratio of transmitted radiant power to incident radiant power. Total transmittance is further subdivided in regular transmittance T_r and diffuse transmittance T_d.

$$T = T_r + T_d \tag{1.15}$$

The present work is focused on thin silicon wafer solar cells and transmission loss is one of the significant factors that must be carefully evaluated. To ensure that all radiation above the bandgap energy is absorbed by the wafer/cell, the standard transmission measurement is important. The equation which helps to ensure zero transmission and maximum absorption in the absorber layer is given as follows in the equation:

$$d_{trans=0} = \frac{1}{\alpha\,(E_g)} \tag{1.16}$$

Where $\alpha\ (E_g)$ is the absorption coefficient of photon energy E_g [122]. All reflectance and transmittance measurements were carried out by Bentham PV300 (UK) instrument.

1.3.4 Electrical characteristics

i. Quantum Efficiency

The probability of an incident photon corresponding to the generation and collection of an electron in the solar cell is called quantum efficiency. It is measured

in terms of current flow across the cell. It can be considered that if one photon contributes to one electron (without any recombination), the maximum value of quantum efficiency (QE) will be 100%. Two types of QE are commonly used, viz. (a) external quantum efficiency (EQE) and (b) internal quantum efficiency (IQE).

ii. External Quantum Efficiency (EQE)

External quantum efficiency (EQE)is the ratio between the numbers of charge carriers collected by the solar cell and the number of incidence photons injected by illumination. It may express as:

$$EQE = \frac{\Delta Jsc}{q\Delta\Phi_\lambda} \tag{1.17}$$

Where J_{SC} is denoted as incremental short circuit current, q is the charge of an electron, incident cumulativephoton flux is $\Delta\Phi_\lambda$ at wavelength λ.

iii. Internal Quantum Efficiency (IQE)

Internal quantum efficiency (IQE) is defined as the probability of entering the photons without any reflectance (R), transmittance (T), and related generation of electrons which is indicated by the current in the external circuit and can be presented as:

$$IQE = \frac{EQE}{1-R(\lambda)-T(\lambda)} = \frac{\Delta J_{sc}}{q\Delta\Phi_\lambda\{1-R(\lambda)-T(\lambda)\}} \tag{1.18}$$

All QE measurements were done by Bentham PV 300 (UK) instrument.

iv. Current-voltage (I-V) measurements

The final step of characterizing a solar cell is the measurement of current-voltage properties under dark and illuminated conditions. The voltage of the device obtained in zero current is called the 'open circuit voltage'(V_{oc}), and the current taken at zero voltage condition is called the 'short circuit current' (I_{sc}). The cell's quality is defined by another important parameter: the 'fill factor (FF). The V_{oc}, I_{sc}, and FF values can

be obtained from the I-V curves, which can give us the overall conversion efficiency of the cell as explained in eq. (1.1).

$$\eta = \frac{V_{oc} I_{sc} FF}{P_{inc}} \tag{1.19}$$

The Air Mass 1.5 (AM 1.5) which is represented by 100 mW/cm^2, is treated as the standard light intensity almost in all solar simulators globally. The temperature of the measurement system was fixed at 27^o C. The current produced by photocarrier generation was measured against a small potential difference across a resistance (r ~10 ohm). The corresponding voltage across the cell was measured by the voltmeter, and a variable electronic load was used to change the voltage across the cell to generate the I-V characteristics [123]. Fill factor (FF) can also be interpreted graphically as the rectangular area ratio under the curve.

$$FF = \frac{I_{mp} V_{mp}}{I_{sc} V_{oc}} \tag{1.20}$$

where,I_{mp} = Maximum current, V_{mp} = Maximum voltage,I_{sc} = Short circuit current, V_{oc} = open-circuit voltage.

The I-V measurements were conducted by Cell Tester CT-50AAA from PET, California, USA instrument.